J. Dairy Sci. TBC
https://doi.org/10.3168/jds.2023-23487

Selective anomer crystallization from aqueous solution: Monitoring lactose recovery under mutarotation limitation via ATR-FTIR and theoretical rate analysis

Ramona Bier,[1] Cornelia Eder,[1] Simon A. Schiele,[1] and Heiko Briesen[1]*
[1]Process Systems Engineering, School of Life Sciences, Technical University of Munich, Gregor-Mendel-Str. 4, 85354, Freising, Germany

ABSTRACT

Lactose is typically produced via cooling crystallization either from whey(-permeate) (edible-grade) or from aqueous solution (pharmaceutical-grade). While in solution, lactose is present in 2 anomeric forms, α- and β-lactose. During cooling crystallization under standard process conditions, only α-lactose crystallizes, depleting the solution of α-anomer. In practice, mutarotation kinetics are often assumed to be much faster than crystallization. However, some literature reports limitation of crystallization by mutarotation. In the present research, we investigate the influence of operating conditions on mutarotation in lactose crystallization and explore the existence of an operation regimen where mutarotation can be disregarded in the crystallization process. Therefore, we study crystallization from aqueous lactose solutions by inline monitoring of concentrations of α- and β-lactose via attenuated total reflection Fourier-transform spectroscopy (**ATR-FTIR**). By implementing a linear cooling profile of 9 K/h to a minimum temperature of 10°C, we measured a remarkable increase in β/α-ratio, reaching a maximum of 2.19. This ratio exceeds the equilibrium level by 36%. However, when the same cooling profile was applied to a minimum temperature of 25°C, the deviation was significantly lower, with a maximum β/α-ratio of 1.72, representing only an 8% deviation from equilibrium.We also performed a theoretical assessment of the influence of process parameters on crystallization kinetics. We conclude that mutarotation needs to be taken into consideration for efficient crystallization control if the crystal surface area and supersaturation are sufficiently high.

Keywords: Lactose, mutarotation, crystallization, ATR-FTIR, FBRM

INTRODUCTION

Lactose is an industrially important disaccharide, serving as a constituent in infant formulae, pharmaceutical tablets, inhalers and processed foods (McSweeney and Fox, 2009). It is produced in the dairy industry by crystallization from whey or whey permeate, both of which are byproducts derived from cheese production. Lactose is composed of galactose and glucose linked by a β1→4 glycosidic bond. Like other sugars, lactose forms a hemi-acetal ring structure in 2 anomeric forms: α-lactose and β-lactose. In solution, the 2 anomers can interconvert via their open-chain form. This equilibrium reaction is called mutarotation (McSweeney and Fox, 2009). The 2 anomers have very distinct properties, e.g., specific optical rotation (Roetman and Buma, 1974; McSweeney and Fox, 2009; Buma and van der Keen, 1974) or solubility (Töpel, 2016; McSweeney and Fox, 2009). Given that the solubility of β-lactose is higher (55 g/100g H2O for β-lactose compared with 8 g/100g H2O for α-lactose hydrate at 20°C) and less temperature-dependent, only α-lactose crystallizes from aqueous solution below 93.5°C in the form of α-lactose monohydrate (Töpel, 2016). The latter is the commercially most available form. α-lactose monohydrate is usually produced from whey or whey permeate via evaporative concentration, batch cooling crystallization, centrifugation, and drying. Edible-grade lactose is produced using a single crystallization step. For pharmaceutical purposes, a second recrystallization step is needed to achieve the required crystal purity (Wong and Hartel, 2014; Paterson, 2016; Wong et al., 2012). For recrystallization, lactose crystals (edible grade) are redissolved in water and impurities are removed via adsorption using activated carbon and batch cooling crystallization. In addition to purity, a narrow monomodal size distribution is also desired. Many dairy manufacturers provide both edible grade and pharmaceutical grade lactose providing lactose products of different specifications. Crystallization is the slowest process involved in production. In many industrial plants, crystallizers are cooled from 65 to 70°C to 15–25°C

Received March 14, 2023.
Accepted September 2, 2023.
*Corresponding author: heiko.briesen@mytum.de

within approximately 12–48 h (Paterson, 2009). In the beginning of the crystallization step, a large number of crystals nucleate during fast cooling. In the case of crystallization from whey or whey permeate, it is assumed that impurities cause heterogeneous nucleation (Wong and Hartel, 2014). In the case of recrystallization, in which only a small quantity of impurities is still present, the addition of seed crystals is necessary to induce secondary nucleation. Relying on primary nucleation would require excessively long induction times (Simone et al., 2019; Raghavan et al., 2001). The goal of effective process control is that, after an initial nucleation event, nuclei and seed crystals should grow. Further secondary nucleation should be minimized to achieve a narrow monomodal crystal size distribution. During crystallization, growth depletes supersaturation of α-lactose, so β-lactose mutarotates to α-lactose to restore mutarotation equilibrium. If the growth kinetics are faster than the mutarotation kinetics, the ratio of β/α-lactose will increase and crystallization will slow because the level of supersaturation is decreasing. However, the literature does not agree on whether or not mutarotation affects lactose crystallization. Haase and Nickerson (1966b) and Herrington (1934a) both concluded that the influence of mutarotation should not be a governing factor in lactose crystallization. Haase and Nickerson (1966b) measured rate constants of both crystallization and mutarotation at different temperatures and compared them to each other. Given that the rate constants of mutarotation were higher than the crystallization rates, they assumed growth to be rate determining. However, mutarotation and growth were measured separately, and rate constants are not really suitable for comparison because the rate of change also depends on the current β/α ratio, supersaturation and crystalline surface area. In an even earlier study, Herrington (1934a) observed very slow growth rates in his studies on primary nucleation of lactose and concluded that mutarotation should not be a limiting factor in crystallization. Other researchers often take on this conclusion (Raghavan et al., 2001; Simone et al., 2019). In their own experiments, Simone et al. (2019) found no significant influence in terms of yield or final crystal size distribution when changing the cooling rate from 9 K/h to 15 K/h. They deduced that, since mutarotation should be affected by changes in cooling rate, growth and secondary nucleation must be even slower than both the cooling rate and mutarotation kinetics. However, Twieg and Nickerson (1968) measured the β/α ratio during crystallizations at constant temperature and varying seed amounts via offline polarimetry and demonstrated an offset of β/α ratio in their experiments with increasing amount of seed crystals. They concluded that mutarotation limits crystal growth, depending on the available growing crystal area. However, only a relatively small range of concentration and temperature was tested. Troy and Sharp (1930) and Mimouni et al. (2009) assumed that mutarotation is also a limiting factor, because they measured faster crystallization rates at a pH level differing from neutral. This was attributed to faster mutarotation rates at pH levels below 2 and above 7 (Troy and Sharp, 1930). However, the pH level can also affect surface integration during growth, so this observation was not entirely conclusive. Rachah and Noll (2015) conducted simulations on the fed-batch crystallization of lactose, which resulted in a shift to β/α ratios of up to 9 at a constant temperature and feed rate. There was no experimental validation of their results. In comparison to experimental results from batch crystallization by Twieg and Nickerson (1968) β/α ratios of up to 9 are extremely high and the results depend on the kinetic parameters of nucleation, growth, and mutarotation that are plugged into the model. Therefore, no clear consensus (derived neither from earlier nor recent research) yet exists on whether or not mutarotation should be considered. The lack of unambiguous research on mutarotation limitation on crystallization has 2 reasons:

A) The influence of mutarotation on crystallization appears to be highly dependent on process conditions. We hypothesize that the choice of process conditions can impact whether or not mutarotation limitation is observed. Table 1 summarizes experimental conditions for the batch cooling crystallization of lactose in previous studies. Isothermal, linear, or piecewise linear cooling profiles have most commonly been applied, with the seed load varying from 0 to 25 wt/wt-%. In the case of piecewise linear cooling a fast cooling step is initially applied to generate a sufficient quantity of nuclei which should subsequently grow during the second slower cooling period. Cooling rates between 1.9 and 25.8 K/h are applied during the slower cooling period. The table illustrates the high variety of process conditions tested.
B) Until now, monitoring β/α ratio inline during crystallization has been challenging. Conventionally, mutarotation is measured via polarimetry (Haase and Nickerson, 1966a; Roetman and Buma, 1974; Buma and van der Keen, 1974; Jawad et al., 2014; Sánchez-García et al., 2021; Troy and Sharp, 1930; Herrington, 1934b; Patel and Nickerson, 1970). The drawback of polarimetry is that it is difficult to measure in turbid solutions, thus, rendering it infeasible for inline monitoring. To measure specific rotation during

crystallization, a representative sample needs to be taken, solids need to be removed via filtration or centrifugation, and the sample must be brought to measurement temperature. Of course, mutarotation continues during sample preparation making measurement by means of offline polarimetry less reliable. Attenuated total reflection Fourier-transform infrared spectroscopy (**ATR-FTIR**) is a popular tool for inline concentration measurement in crystallization experiments and it is able to measure in turbid solutions (Frawley et al., 2012; Nagy and Braatz, 2012; Woo et al., 2009; Cornel et al., 2008; Nagy et al., 2008; Zhou et al., 2006; Fujiwara et al., 2002; Lewiner et al., 2001). We have in recent research demonstrated that ATR-FTIR spectroscopy is capable of inline measuring the mutarotation state (Schiele et al., 2020). However, the method was only applied to clear lactose/water mixtures and dissolution at low concentrations. It has not yet been applied to crystallization process monitoring.

Based on statement A), we infer that the impact of mutarotation on the crystallization depends on the process conditions applied. We assume that there is no general answer as to whether mutarotation should be considered during crystallization, and hence, our focus is to ascertain the process conditions under which mutarotation should be considered. The present research article aims to exploit the capability of inline anomer concentration measurement to elucidate the influence of mutarotation on crystallization. This study contributes to developing a better understanding of the mechanistic interactions involved in the crystallization process. This improved process understanding is crucial for optimizing production efficiency in the dairy industry. Experiments and theoretical analysis were conducted regarding lactose in water. Therefore, the results are transferable to the recrystallization step during the production of pharmaceutical-grade lactose. The kinetics are different in the case of crystallization from whey or whey permeate, so a general assessment is not possible as it would also depend on the solution composition. Nevertheless, if the composition and kinetics of the incoming process stream (sweet/ acid whey or whey permeate) are known, the rate analysis can be applied in a similar manner. The present article is organized as follows:

I) Commonly applied crystallization process parameters were experimentally tested, and mutarotation state was monitored inline. II) The influence of process parameters was assessed theoretically and compared with the experimental results.

MATERIALS AND METHODS

Lactose solution composition is reported as loadings, i.e., as mass of anhydrous lactose per mass of water, if not explicitly stated otherwise. Demineralized water was used for all experiments.

MATERIALS

Pharmaceutical-grade α-lactose monohydrate (purity $\geq$ 99%, $\geq$ 96% α-lactose) from Sigma Aldrich Inc., U.S.A., and β-lactose from Acros Organics B.V.B.A. ($\geq$80% β-lactose) were used for all calibration experiments. For crystallization experiments coarse pharmaceutical-grade α-lactose monohydrate (purity $\geq$99.9%) was supplied by Meggle GmbH & Co. KG (Wasserburg, Germany) with the tradename SpheroLac 100. The anomer content in the lactose was determined using polarimetry. A detailed description of the method can be found in the appendix."

The experiments were conducted in a Mettler Toledo OptiMax 1001 reactor with 500 mL reactor vessel volume controlled by iControl 6.1. A pitched-blade up impeller (45 ° angle, 4 blades) was used to stir the reactor contents at 500 rpm (Re $\approx 10^4$, tip velocity u = 1.18 m/s). A Mettler Toledo, Inc. U.S.A, ReactIR 15 spectrometer with a liquid nitrogen MCT detector and a DST AgX DiComp 9.5 mm probe was used for ATR-FTIR measurements. The spectrometer is controlled via iC IR 7.1 software. Spectra were collected at a resolution of one measurement per 4 wavenumbers in the range of 800–2000 cm^{-1} and averaged over 122 scans within 45 s. Before each experiment a new background was collected while the probe was already positioned in the reactor and the reactor was still empty and dry. A ParticleTrack G400, focused beam reflectance measurement (**FBRM**) probe with iC FBRM software (version 4.4) from Mettler Toledo was used for tracking crystal population evolution. Software settings for FBRM data were macro, no weight. Measurement interval was set to 10 s. The total particle counts and chord length distributions were obtained inline, based on FBRM measurements. Total particle counts were used to detect changes in particle numbers due to, e.g., nucleation or agglomeration.

ATR-FTIR – CALIBRATION MEASUREMENTS

Samples were taken at least every hour during the ATR-FTIR calibration experiments, and the concentration was measured using refractometry. Calibration spectra were obtained in the range of 0.07–1.3 g/g and 10–90°C. The calibration measurements and the model built are described in detail in the appendix.

Table 1: Summary of experimental conditions in literature for batch cooling crystallization of lactose

Reference	Composition	Lactose concentration (anhydride) [g/ g H_2O]	Seed load [wt/wt-% of initial dissolved lactose]	Temperature profile
Darmali et al. (2021)	Lactose - water Model solution of 1 wt/wt-% whey protein at pH 4.5 adjusted with either lactic acid or acetic acid	0.82	4	T_{seed} = 76°C (saturation temperature) T_{seed} → 20°C at 15 K/h; 2 h at 20°C
Wijayasinghe et al. (2020)	Lactose – water Model solution with 1:100, 1:5 and 4:5 lactic, citric or phosphoric acid ratio to lactose	0.91 (for pure lactose)	(Primary nucleation)	T_{Ini} = 55°C (saturation temperature) T_{Ini} → 30°C at 150 K/h; 2 h at 30°C; 30°C → 15°C at 5 K/h Kept overnight at 15°C
Simone et al. (2019)	lactose -water	0.45–0.55	0.1–2	T_{seed} = 45.5/50.5°C T_{seed} → 6°C at 9/15 K/h Hold at 6°C Total duration 24 h
Pandalaneni and Amamcharla (2018)	Milk permeate and deproteinized whey permeate	1.02 (deproteinized whey) 1.10 (milk permeate)	(primary nucleation)	T_{Ini} = 80°C T_{Ini} → 60°C at 30 K/h; 60°C → 20°C at 2.4/3.6/4.8 K/h
Chandrapala et al. (2016)	Model solution with 1:5, 3:25, 2:25, 1:25 lactic acid to lactose or 1:42, 1:69 calcium to lactose	0.70–0.86	(primary nucleation)	T_{Ini} = 55°C T_{Ini} →30°C rapidly; 30°C → 15°C at 4.8 K/h Kept overnight at 15°C
Pandalaneni and Amamcharla (2016)	lactose - water	1–1.5	(primary nucleation)	T = constant T = 20 / 30°C
Gernigon et al. (2013)	lactose – water Model solutions with addition of various organic salts, galactose, protein	0.7	(primary nucleation)	T = constant T = 30°C
Wong et al. (2012)	Lactose - water	0.58	About 0.02–0.04 (25 mg of seeds with exact initial lactose amount not given)	T_{seed} = 76.5°C T_{seed} → 25/30°C at 25.8/3.3/1.9 K/h
Mimouni et al. (2009)	lactose - water	0.55/0.69/0.80 for unseeded experiments 0.7 for seeded experiments	14	T = constant T = 25/30°C
Vu et al. (2006)	lactose - water	0.63	2.6–3.9	T = 70–10°C; Different cooling profiles; Total duration 25 h
Raghavan et al. (2001)	lactose – water	0.44–0.58	(primary nucleation)	T = constant T = 31/40/20°C
Zeng et al. (2000)	lactose – water	0.49/ 0.75/ 1/ 1.5	(primary nucleation)	T = constant T = 0/40°C
Twieg and Nickerson (1968)	lactose – water	0.27- 0.6	0.29–25	T = constant T = 4/14/25°C Total duration 4–20 h
Haase and Nickerson (1966b)	lactose – water Concentrated whey	0.45–0.52 (pure lactose solutions)	Not stated	T = constant T = 0.5/15/25°C

In short, a partial least-squares multivariate regression (**PLS**) using the calibration spectra was performed using the iCQuant software package (Mettler Toledo Inc., U.S.A.). 75% of the calibration data were taken as a training set, and 25% as a test set. A 5-fold cross validation was performed by leaving out 20% of the training set. The regression was performed on the spectral region of 1200–950 cm^{-1}. The respective correlation coefficients obtained were: R^2 of 0.998 for α-lactose and 0.998 for β-lactose and a RMSEP of 0.008 mol/L and 0.010 mol/L. The molar concentrations were calculated to loads as described in the appendix.

CRYSTALLIZATION EXPERIMENTS

Solutions for crystallization were prepared by dissolving α-lactose monohydrate at 80°C and cooling them to the starting temperature T_{seed}. 50–90 μm sieve fraction of SpheroLac 100 crystals were used as seed crystals. For crystallization, the suspension was cooled according to the chosen temperature profile. Crystallization was carried out for 24 h in each run. Two commonly applied strategies for crystallization experiments were tested: A) a fast cooling step for generation of secondary nuclei was coupled with a subsequent slow linear cooling profile. A small quantity of seeds is used at 0.63 g/g starting load, and a quick first cooling step for the generation of nuclei was applied followed by slow cooling to final temperature. The temperature profile chosen was similar to those of Chandrapala et al. (2016), Wijayasinghe et al. (2020), and Pandalaneni and Amamcharla (2016) (see Table 1). B) A cooling profile at a constant cooling rate was used. For the fast cooling profile, the solutions were seeded with 3 wt.% and a 9 K/h linear cooling profile starting from 0.45 g/g load was adapted based on experiments by Simone et al. (2019). However, the final temperature was chosen differently. For strategy B), 10°C and 25°C were tested as the final temperature. Each run was performed in triplicate. The experimental conditions are shown in Table 2. During preliminary experiments, it was observed that lactose crystals tend to deposit and grow on the ATR-FTIR window regardless of stirrer speed or probe positioning. Heating the probe tip was found to be efficient in preventing excessive probe fouling. A heating wire electrically insulated with a microfluidic tube was wrapped around the probe tip, further thermally insulated from the surrounding media and powered by a Philips N.V. PE 1512 laboratory power supply. Fifteen W were found to be sufficient for heating the probe tip. Nevertheless, slight particle depositing could not be prevented at high solid concentrations which occurred at the end of experiments. Periodic cleaning in place (**CIP**) was performed via reduction of stirrer speed to 100 rpm for up to 5 min. This resulted in a steep increase in temperature at the probe tip and quick dissolution of deposited solids. Effect of CIP procedure on crystallization is discussed in the appendix. In summary, no significant influence of CIP on crystallization could be detected. However, ATR-FTIR and FBRM-measurements are not reliable during CIP. Consequently, measurement data during CIP or probe fouling were excluded from the results. This results in a non-uniform distribution of data in addition to noise-contaminated data values. Therefore, Tikhonov regularization, as described in Knowles and Renka (2014), was performed on concentration data, α-lactose mass fraction and FBRM counts with regularization parameter 10^{13} and a subinterval length of 44 s. The regularized data were then averaged over all 3 repetitions.

THEORETICAL RATE ANALYSIS

Throughout our experiments, we sought to evaluate mutarotation under common process conditions. However, unless extensive experimental effort is undertaken, a general prediction of mutarotation limitation is difficult using experiments alone. A mechanistic approach was performed to analyze the impact of process conditions and enable prediction of the mutarotation effect under various parameter combinations. This theoretical assessment enabled us to evaluate mutarotation limitation at fixed time points and system states. We derive our theoretical assessment as follows: The governing kinetics influencing the β/α ratio are mutarotation

Table 2: Experimental conditions given with standard deviations of 3 repetitions

Experiment No.	Initial lactose concentration [g/g H2O]	Seed load [wt/wt-% of initial dissolved lactose]	Temperature profile
1 – 2-step cooling	0.63 ± 0.01	0.065 ± 0.003	T_{seed} = 60°C 60°C → 40°C in 20 min 40°C →10°C at 2 K/h
2 – fast linear	0.45 ± 0.01	3.22 ± 0.02	T_{seed} = 45.5°C 45.5°C →10°C at 9 K/h
3 – fast linear to 25°C	0.45 ± 0.01	3.20 ± 0.01	T_{seed} = 45.5°C 45.5°C →25°C at 9 K/h

and growth rate because they both affect α-lactose concentration. The change in α-lactose concentration is described by the following differential equation:

$$\frac{dc_\alpha}{dt} = \left(\frac{dc_\alpha}{dt}\right)_G + \left(\frac{dc_\alpha}{dt}\right)_M. \quad (1)$$

The first term represents the depletion of dissolved α-lactose by crystal growth, and the second part represents the change in α-lactose load by mutarotation kinetics. We do not solve this differential equation for a given time line as doing so would involve setting up and parametrizing a full population balance model, including nucleation and agglomeration. Instead, we calculated the rate under fixed system states to perform our rate analysis. The 2 terms are calculated as follows: Mutarotation drives the lactose anomers toward their thermodynamic equilibrium via a first-order reversible reaction:

$$\alpha \underset{k_2}{\overset{k_1}{\rightleftarrows}} \beta \quad (2)$$

with k_1 and k_2 being the rate constants (Haase and Nickerson, 1966b). The rate of mutarotation highly depends on temperature, pH and the salts present in solution (Troy and Sharp, 1930; Herrington, 1934b; Patel and Nickerson, 1970; Schiele et al., 2020). The mutarotation rate can be calculated according to Equation (3).

$$\left(\frac{dc_\alpha}{dt}\right)_M = -k_1 c_\alpha + k_2 c_\beta. \quad (3)$$

For constant total lactose load, mutarotation kinetics can be written as:

$$\frac{dx_\alpha}{dt} = -k_1 x_\alpha + k_2\left(1 - x_\alpha\right), \quad (4)$$

with x_α being the mass fraction of α-lactose based on total lactose dissolved. This equation can be easily integrated to

$$x_\alpha(t) = \left(x_{\alpha,0} - x_{\alpha,eq}\right)e^{-\frac{t}{\lambda}} + x_{\alpha,eq} \quad (5)$$

following the proposed nomenclature of Schiele et al. (2020) $k_1 + k_2 = \frac{1}{\lambda}$ and $x_{\alpha,0}$ being the initial α-lactose fraction and $x_{\alpha,eq}$ the fraction of α-lactose in equilibrium. McLeod (2007) provides an empirical correlation for the temperature T dependency of β/ α ratio for pure lactose-water solutions.

$$K(T) = \frac{x_{\beta,eq}}{x_{\alpha,eq}} = \frac{k_1}{k_2} = 1.6353 - 0.0024\frac{1}{[°C]}\cdot\left(T - 273.15°C\right) \quad (6)$$

Furthermore, McLeod (2007) fitted an Arrhenius approach to the data of Haase and Nickerson (1966a), Haase and Nickerson (1966b), van Krevald (1969) and Kendrew and Moelwyn-Hughes (1940) to obtain a correlation for the mutarotation coefficient k_1.

$$k_1 = 2.25\cdot 10^8 \frac{1}{s}\cdot\exp\left(\frac{-68.46\frac{\text{kJ}}{\text{mol}}}{RT}\right) \quad (7)$$

Using Equation (6) k_2 can also be easily evaluated.

Depletion rate by growth can be calculated according to the following equation including change of water mass due to hydrate formation:

$$\left(\frac{dc_\alpha}{dt}\right)_G = \frac{1}{m_{H2O}}\cdot\frac{dm_{Lac}}{dt} + m_{Lac}\cdot\frac{dm_{H2O}^{-1}}{dt}. \quad (8)$$

This rate describes the overall depletion of lactose by crystal growth which we consider equivalent to the consumption of α-lactose. This is a common assumption, because, during cooling crystallization below 93.5°C, α-lactose monohydrate is the predominant form (Töpel, 2016). In a recent study by Simone et al. (2019), the α- and β-lactose percentages were determined in lactose crystals after cooling crystallization experiments using H-NMR. They observed a maximum percentage of 3% for β-lactose. In the study by Altamimi et al. (2019), the anomer content of commercially available α-lactose hydrate was analyzed. The findings revealed an average β-lactose content of 2.6% in the α-lactose monohydrate produced by Meggle GmbH using crystallization, followed by sieving or milling. Therefore, the incorporation of β-lactose was deemed negligible in the rate analysis. The change in lactose and water mass can be calculated as deduced from the standard method of moments (Gernigon et al., 2013):

$$\frac{dm_{Lac}}{dt} = -3G\cdot\mu_2\cdot k_v\cdot\rho_{Cryst}\cdot 0.95 \quad (9)$$

$$\frac{dm_{H2O}}{dt} = -3G\cdot\mu_2\cdot k_v\cdot\rho_{Cryst}\cdot 0.05, \quad (10)$$

where G is the mean crystal face growth rate, μ_2 represents the second order moment of the crystal population representing a measure for the total surface area available for growth. k_V and ρ_{Cryst} are the volume shape factor and the crystal density, respectively. The factors 0.95 and 0.05 account for the fact that α-lactose monohydrate is crystallized, with 95 wt/wt% being lactose and 5 wt/wt% being water. The growth rate of the (010) surface of an α-lactose crystal as a function of α-lactose concentration and temperature was determined as described in the appendix and was used as the mean crystal face growth rate.

$$G = 6.80 \cdot 10^{15} \frac{\mu m}{h} \cdot \exp\left(\frac{-87 \frac{kJ}{mol}}{RT}\right) \cdot S^{1.8} \tag{11}$$

Supersaturation S is defined as follows:

$$S = \frac{c_\alpha}{c_{\alpha S}} - 1, \tag{12}$$

with $c_{\alpha S}$ being the saturation concentration of α-lactose according to Visser (1982).

$$c_{\alpha S} = c_{\alpha S,eq} - F\left[c_\beta - K c_{\alpha S,eq}\right] \tag{13}$$

$$c_{\alpha S,eq} = \frac{c_S}{K+1} \tag{14}$$

$$F = 0.0187 \cdot \exp\left(\frac{0.0236\left(T - 273.15\right)}{\left[°C\right]}\right) \tag{15}$$

F is thereby a factor for the depression of solubility of α-lactose in the presence of β-lactose. Solubility is calculated based on the equation provided by McLeod (2007):

$$\frac{c_S}{\left[\frac{g}{100g}\right]} = 10.9109 \cdot \exp\left(0.02804 \cdot \frac{T - 273.15}{\left[°C\right]}\right). \tag{16}$$

By using these equations, we can establish a ratio of rates that indicates whether the process moves closer to or further away from the mutarotation equilibrium. This ratio describes how the α-lactose changes relative to a hypothetical rate of change that maintains a constant β/α ratio:

$$\kappa_r = \frac{\left(\frac{dc_\alpha}{dt}\right)}{\left(\frac{dc_\alpha}{dt}\right)_{x_\alpha = const.}} = \frac{\left(\frac{dc_\alpha}{dt}\right)_G + \left(\frac{dc_\alpha}{dt}\right)_M}{x_\alpha \cdot \left(\frac{dc_\alpha}{dt}\right)_G} = \frac{1}{x_\alpha} + \frac{\left(\frac{dc_\alpha}{dt}\right)_M}{x_\alpha \cdot \left(\frac{dc_\alpha}{dt}\right)_G}. \tag{17}$$

In other words, the denominator is the maximum possible depletion of α-lactose without changing the β/α ratio. Note that $\left(\frac{dc_\alpha}{dt}\right)_G$ is in general negative while $\left(\frac{dc_\alpha}{dt}\right)_M$ is mostly positive during crystallization. The correlation between mutarotation, growth and β/α ratio for different κ_r is also demonstrated graphically in Figure 1. A κ_r smaller than 0 indicates a higher mutarotation rate than growth rate. In that case, α-lactose load will actually increase while β-lactose load will decrease, and the β/α ratio decreases. In the second scenario of Figure 1, the kinetic ratio is 0, and the α-lactose load remains constant, which can only occur (at a nonzero growth rate) if the mutarotation rate equals the growth rate. The β-lactose load will then decrease and the β/α ratio decreases. A κ_r larger than 0 needs to be evaluated for separate cases. Two cases represent a higher growth rate than mutarotation rate. However, the extent of mutarotation rate in comparison to the growth rate determines whether β/α ratio is increasing, decreasing or remains constant. The latter is the case if κ_r equals 1. A κ_r larger than 1 but smaller than $\frac{1}{x_\alpha}$ means that mutarotation rate is very small relative to growth depletion rate, and the β/α ratio is increasing. While at κ_r smaller than 1 mutarotation rate is only slightly smaller than the growth rate, resulting in a large drop in β-lactose concentration, so β/α ratio decreases. In the last case, κ_r is even larger than $\frac{1}{x_\alpha}$, which can only be the case if the mutarotation rate is moving toward β-lactose, so $\left(\frac{dc_\alpha}{dt}\right)_M$ is negative. In summary, if the kinetic ratio is larger than 1, then the β/α ratio is increasing. While at ratios smaller than 1, the β/α ratio decreases. From the equations above, the governing process variables can be derived: x_α, S, T, μ_2. A parameter variation was performed to quantitatively evaluate their influence on the kinetic ratio. For simplicity, a mono-sized cube-shaped crystal population of 50 μm is assumed. In this scenario, enlarging the surface area of the crystals is equivalent to increasing the quantity of crystals within the system. Therefore, crystal surface area can be easily calculated from specific surface area and scales linearly with crystal mass. We will use the

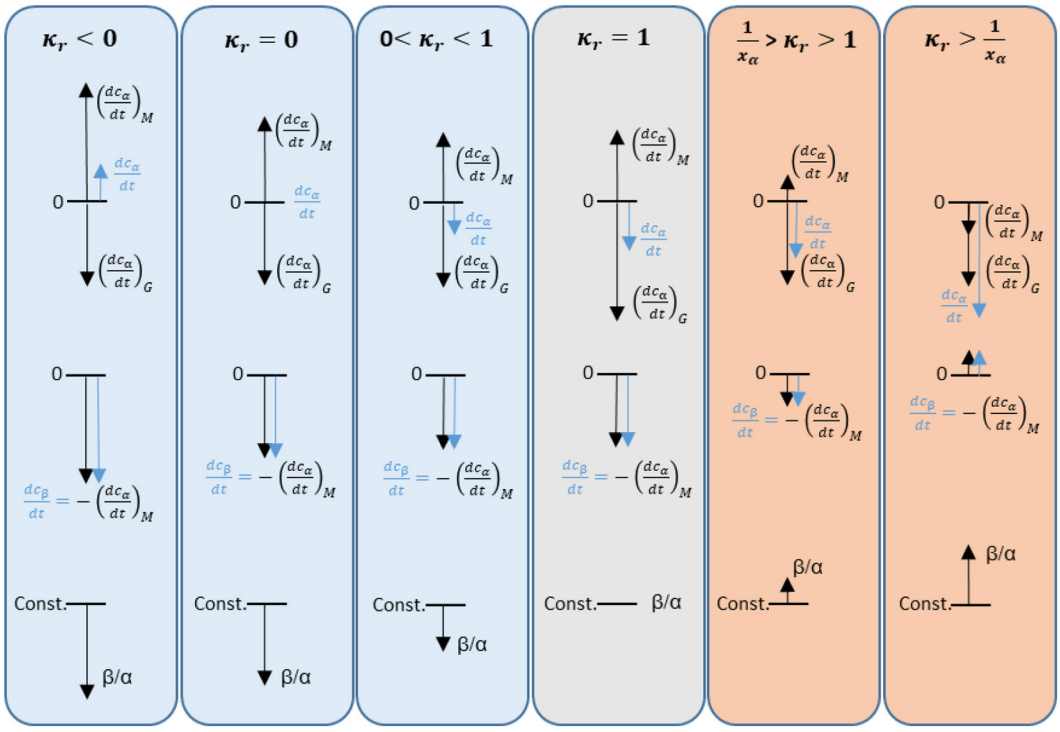

Figure 1. Scheme showing the correlation of mutarotation, growth and β/α ratio in dependence of the kinetic ratio κ_r. Length of arrows represent extent and orientation the mathematical sign (+/−) of mutarotation (M) and growth (G) in each scenario as well as overall rate in blue.

mass of crystals per mass of water (crystal load) instead of surface area in our evaluation. Of course, during crystallization specific surface area changes in general as crystals grow and nucleation occurs. However, for the evaluation of the kinetic ratio and development of β/α ratio at different system states this simplified consideration was deemed sufficient.

RESULTS AND DISCUSSION

Crystallization results

Inline measurements. The results from the 3 process parameter settings described in Table 2 are shown in Figure 2Figure 4. In addition, the degree of supersaturation was computed and plotted assuming equilibrium and using the measured fraction of α-lactose. When comparing the measured α-lactose fraction to its equilibrium value, differences up to 0.07 ($x_{\alpha,eq} = 0.38$) were observed in 2 step-cooling and fast cooling to 10°C and 0.02 ($x_{\alpha,eq} = 0.39$) in fast cooling to 25°C. This deviation from equilibrium demonstrated that the mutarotation kinetics were slower than growth and nucleation. Ideally, α-lactose is depleted via growth during crystallization, and β-lactose mutarotates to the α-form and maintains mutarotation equilibrium. However, since α-lactose fraction was measured as having decreased, the mutarotation rate was obviously slower during part of the experiment under all of the tested process conditions. The β/α ratio increased and supersaturation decreased as less α-lactose was available. We calculated a maximum deviation in actual supersaturation compared with the supersaturation calculated from equilibrium of 0.33 (58%) in 2 step-cooling, 0.47 (44%) in fast cooling to 10°C and 0.09 (13%) in fast cooling to 25°C. The trajectories of the α-lactose fraction were distinctly different in all of the experiments, thus demonstrating the influence of process conditions on kinetics and their interplay. In 2 step-cooling, the first cooling step resulted in a quick rise in supersaturation, and FBRM total counts started to rise. After 4 h, the secondary nucleation rate increased as indicated by total counts. Subsequently, a large crystal surface area was available for growth which led to a decrease in both the lactose load and the fraction of α-lactose. A minimum in α-lactose fraction was reached at around 16 h. Afterward, α-lactose fraction started to increase gradually, which can be attributed to slow growth resulting from the low degree of supersaturation. If equilibrium were maintained throughout the experiment, then supersaturation should actually increase again between 8 and 16 h. Regarding fast cooling to 10°C, the results showed a qualitatively similar behavior to the first scenario, but the minimum of α-lactose mass frac-

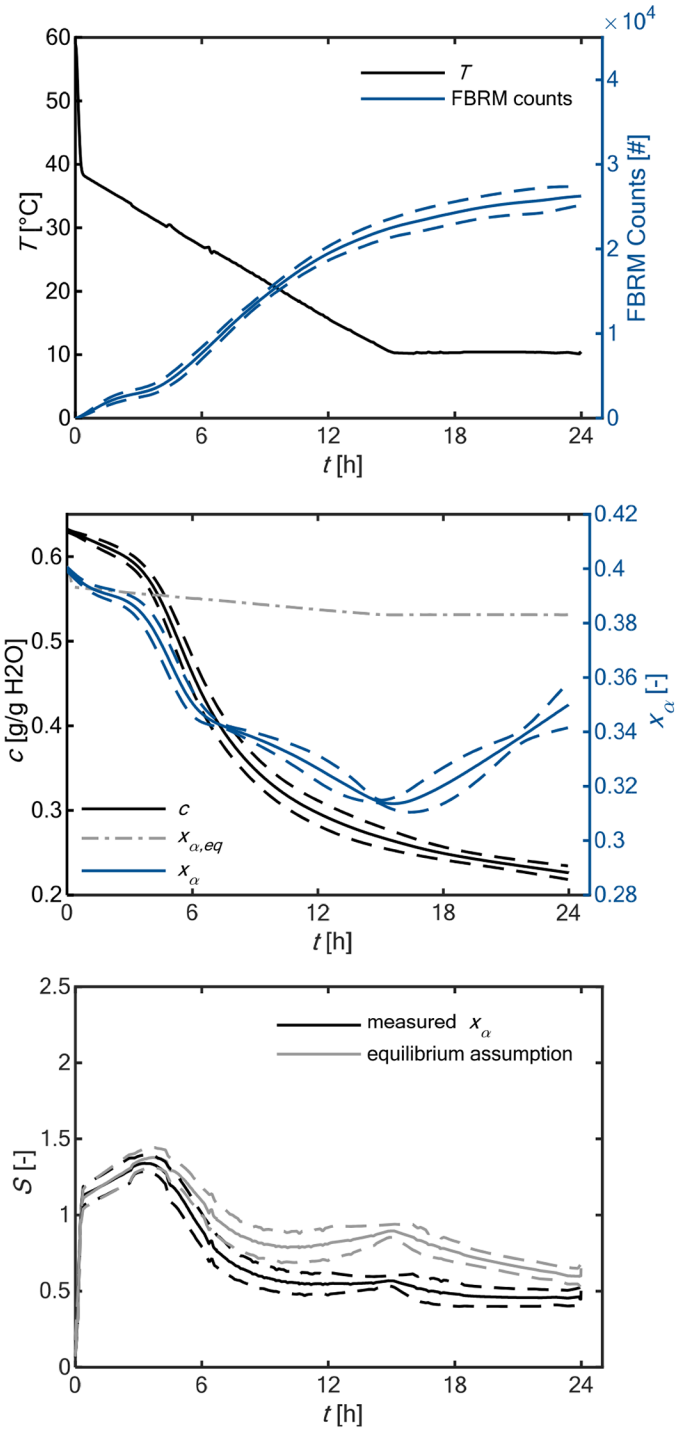

Figure 2. From top to bottom: 1) Temperature profile and focused beam reflectance measurement (**FBRM**) total counts, 2) Lactose load c and α-lactose mass fraction x_α and 3) supersaturation S with measured α-lactose fraction and calculated with equilibrium assumption for experiment 1. Averaged profiles over 3 repetitions are shown with standard deviations indicated as dashed lines.

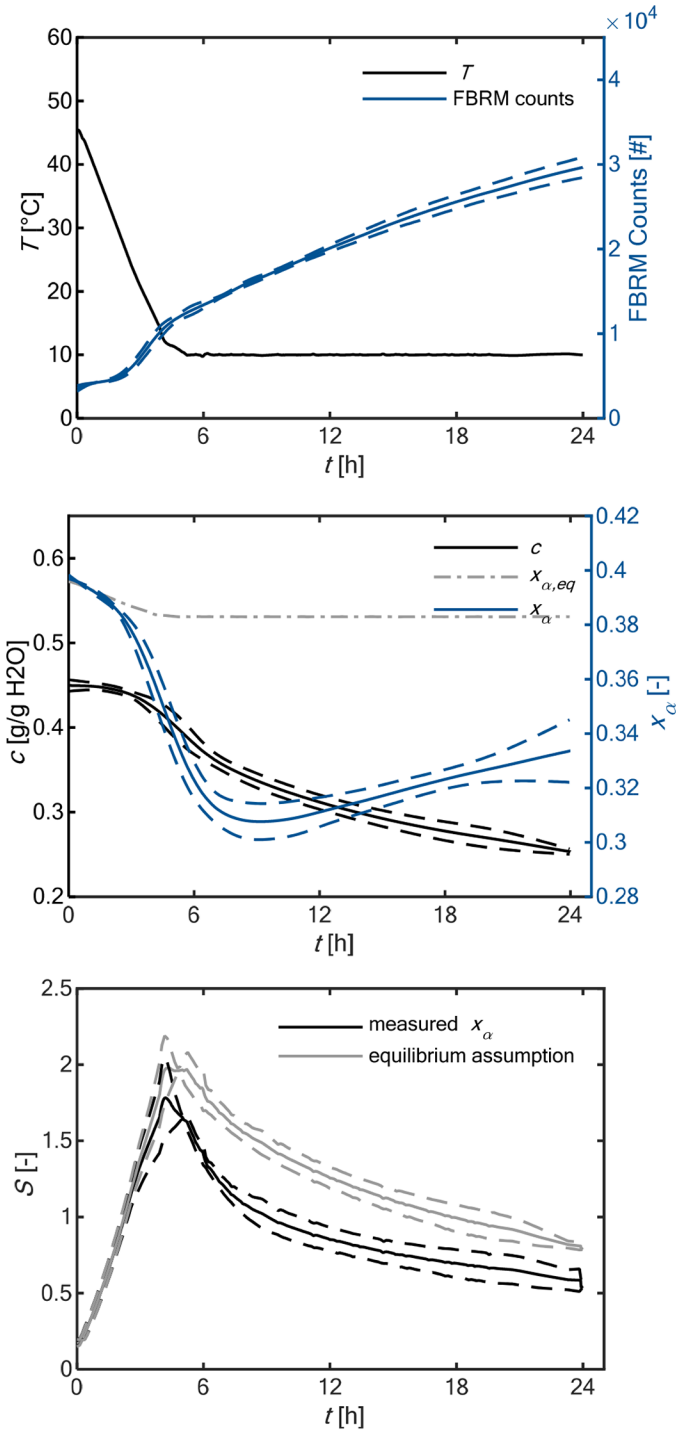

Figure 3. From top to bottom: 1) Temperature profile and focused beam reflectance measurement (**FBRM**) total counts, 2) Lactose load c and α-lactose mass fraction x_α and 3) supersaturation S with measured α-lactose fraction and calculated with equilibrium assumption for experiment 2. Averaged profiles over 3 repetitions are shown with standard deviations indicated as dashed lines.

Table 3: Final yield with standard deviations from 3 repetitions

Experiment no.	Y [%]
1 – 2-step cooling	64.9 ± 1.4
2 – fast cooling to 10°C	44.3 ± 0.6
3 – fast cooling to 25°C	38.7 ± 1.1

tion was reached even more quickly. This observation is consistent with the higher degree of supersaturation observed during the first half of the experiment, which can be attributed to faster cooling, as the absolute lactose load was lower in scenario 2. In the third test scenario, final temperature was set to 25°C, with the seed quantity and temperature ramp being identical to the fast cooling profile. It can be seen that FBRM counts ultimately appeared to be slightly lower than at 10°C final temperature and close to the first scenario. However, the α-lactose fraction only deviated from equilibrium by up to 0.02 ($x_{\alpha,eq} = 0.39$), as opposed to 0.07 ($x_{\alpha,eq} = 0.38$) for the other temperature. Therefore, the mutarotation limitation only slightly affected crystallization in comparison to the first 2 scenarios. There are 2 possible explanations for this outcome: either the higher temperature resulted in faster mutarotation kinetics or the lower degree of supersaturation led to a lower growth rate. The latter explanation seems plausible given that mutarotation limitation was actually observed quite early at high temperatures during the 2 step-cooling scenario. In summary, a complex interplay was observed among mutarotation, growth, and secondary nucleation. Supersaturation is the driving force behind crystallization and will be greatly overestimated by an equilibrium assumption. However, as hypothesized earlier, the influence of mutarotation greatly depends on process conditions. A low degree of supersaturation (e.g., due to higher temperatures or slow cooling) results in slow growth, whereas the mutarotation rate remains unaffected by the degree of supersaturation. Consequently, the α-lactose fraction remains in proximity to equilibrium. Simultaneously, crystal surface area links the face-specific growth rate to concentration depletion rate. At the beginning of crystallization high face-specific growth rates do not result in a substantial rise in β/α ratio, because little crystal surface area is available. A significant increase in the β/α ratio is not observed until secondary nucleation increase crystal surface area. In measurements, therefore, an alignment between a steep rise in FBRM total counts and a decrease in α-lactose fraction was detected.

Yield. To compare the experiments further, final yield was calculated as:

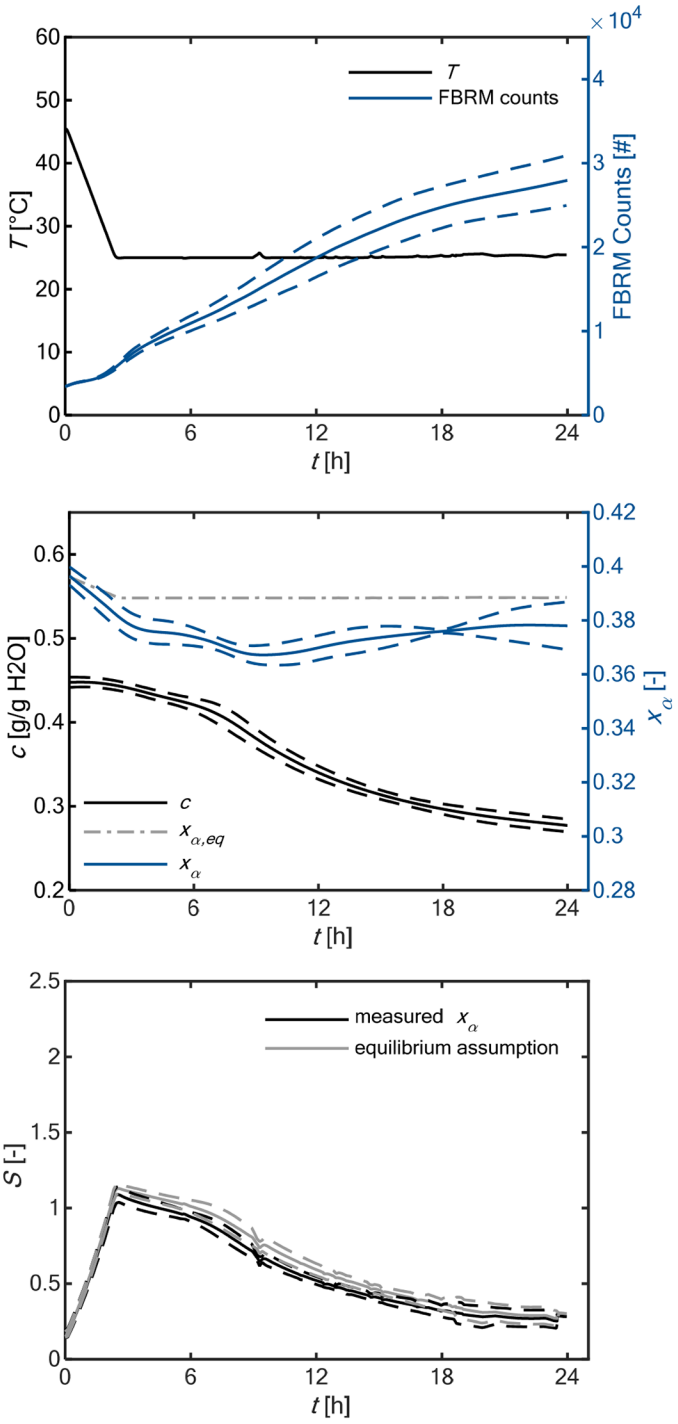

Figure 4. From top to bottom: 1) Temperature profile and focused beam reflectance measurement (**FBRM**) total counts, 2) Lactose load c and α-lactose mass fraction x_α and 3) supersaturation S with measured α-lactose fraction and calculated with equilibrium assumption for experiment 3. Averaged profiles over 3 repetitions are shown with standard deviations indicated as dashed lines.

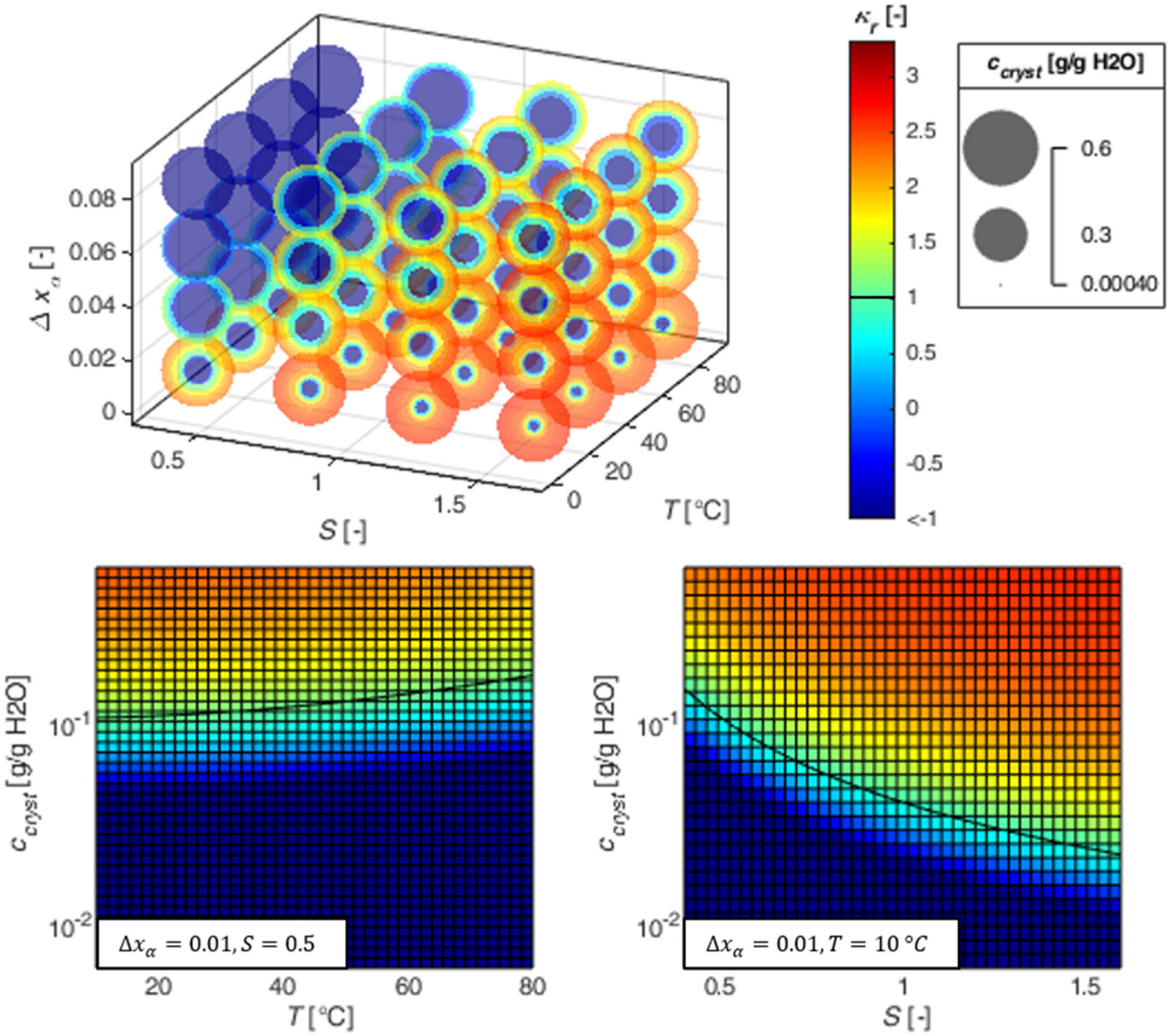

Figure 5. Kinetic ratio κ_r as a function of distance from mutarotation equilibrium Δx_α, crystal load c_{cryst}, temperature T and supersaturation S for a mono-sized cube-shaped crystal population of 50 µm. The position of the bubbles in the 3D plots determines system parameters Δx_α, S, T. Moving from the center outwards of each bubble, the crystal load increases. The color of the bubble at the different radii gives the kinetic ratio. Bottom: 2D surface plots for left: constant supersaturation $S = 0.5$ and right: constant temperature $T = 10°C$ at $\Delta x_\alpha = 0.01$. The black line marks a kinetic ratio of 1.

$$Y = \frac{\text{mass of lactose crystallized}}{\text{total mass of lactose}}. \quad (18)$$

The detailed calculation is given in the appendix. The results are summarized in Table 3 for all experiments. The yield was lowest in fast cooling to 25°C at 38.7%. Although mutarotation limits crystallization at fast cooling to 10°C a higher yield of 44.3% was achieved. The first experiment achieved the highest yield with 64.9%.

Rate analysis

Parameter study. We have thus far demonstrated that mutarotation slows crystallization kinetics. To systematically assess the influence of process conditions on mutarotation in crystallization, we performed

a case study using the approach described in section 2.4. The results are plotted in Figure 5. A bubble chart with a colormap is used to illustrate the 4 dimensional dependency (T, S, Δx_α, c_{cryst}). The size of the bubble scales linearly with crystal load, while the kinetic ratio scales with the colorbar. Two-dimensional plots with 2 constant properties are given as well. When the kinetic ratio exceeds 1, there is an increase in the β/α ratio. It is evident from Figure 5 that the kinetic ratio was considerably affected by the crystal load (size of the bubbles) and degree of supersaturation (x-axis). Temperature (y-axis) as a factor for enhancing the rate constants was less significant. As shown in Figure 5, little influence of temperature (z-axis) on kinetic ratio was observed at constant supersaturation between 10 and 40°C, which was in apparent contrast to the experiments. Experiment 3 (rapid cooling to 25°C) showed minimal mutarotation limitation. However, the degree of supersaturation was simultaneously decreased owing to the increased saturation solubility. The alteration in the kinetic ratio was not due to temperature but rather resulted from a lower degree of supersaturation compared with the other 2 experiments. The low impact of temperature can be explained by comparing the 2 activation energies for mutarotation (7) and growth kinetics (11) because both values fall within a very similar range, and the influence of temperature on equilibrium constant K is small. Therefore, the rate changes in both kinetics are very similar as a function of temperature. Moreover, the secondary nucleation rates were lower when cooling to 25°C, which led to less available crystal surface area. Twieg and Nickerson (1968) already concluded that the impact of mutarotation on crystallization depends on crystal surface area. They even stated that a large enough surface area will result in mutarotation being the rate limiting step. Mutarotation being the rate limiting step would mean that overall lactose depletion rate would be governed by mutarotation kinetics alone and α-lactose fraction would be approximately constant as well as very low. However, in the beginning mutarotation limits growth before that through a decreased supersaturation since less α-lactose is available for crystallization. Our findings support that the crystal surface area largely influences whether mutarotation has an impact on crystallization. Therefore, not only growth, but also nucleation, abrasion, and agglomeration will influence whether mutarotation equilibrium is maintained throughout the process since these phenomena all affect crystal surface area. However, the degree of supersaturation is equally important. At low supersaturation, growth rate is very low whereas mutarotation does not depend on supersaturation. During our experiments, mutarotation did not become the rate limiting step because the α-lactose fraction was constantly changing throughout the experiment. Based on Figure 5, mutarotation is unlikely to become rate limiting unless very high supersaturations are maintained throughout the whole experiment. Of course, a corresponding analysis for the initial crystallization step in dairy manufacturing is of interest, as well. Patel and Nickerson (1970) observed a significant increase in mutarotation rate in model whey solutions prepared following Jenness and Koops (1962) method. The mutarotation velocity increased 1.8–1.9 times in comparison to its velocity in water. However, Jenness and Koops′ model solution replicates the composition of whey permeate obtained after cheese production. Before crystallization, this solution undergoes concentration through evaporation, leading to a substantial increase in salt concentration. Therefore, the results of Patel and Nickerson (1970) are not directly applicable. Haase and Nickerson (1966b) used the same method for solution preparation but concentrated their solution to study mutarotation and crystallization in concentrated model whey solutions. They found a significant increase of mutarotation rate in concentrated whey as well. Consequently, one might hypothesize that mutarotation limitation is less prominent in whey crystallization. However, it is anticipated that the growth rate will differ between whey permeate and pure lactose-water solutions. If the growth rate is higher in whey permeate, it could potentially counterbalance the accelerated mutarotation rate. Therefore, it is necessary to determine the kinetics of growth and mutarotation in concentrated whey and whey permeate to evaluate mutarotation limitation.

Experimental rates. The kinetic ratios throughout the experiments were also calculated, as plotted in Figure 6. Note that the relevant process parameter is the crystal surface area instead of the crystal load. However, the latter is hard to measure during the experiments. To assess the crystal population accurately, particle size and shape measurements must be conducted during the crystallization. In-line (Huo et al., 2020; Schiele et al., 2023), online (Borchert and Sundmacher, 2012; Binel et al., 2023; Lins et al., 2022), and off-line (Neoptolemou et al., 2022; Schiele et al., 2021; Höving et al., 2023) shape and size measurement techniques exist, but are mostly applied to exemplary material systems. Reliable shape measurements of crystals remain a challenge. Nevertheless, the crystal habit and size have an impact on the trajectories in the bubble plots, and because crystal load is used instead of surface area, the theoretical analysis and experiments can only be compared qualitatively. The depiction of the experiments in the bubble plots mirrors our theoretical assessment. A high level of supersaturation was encountered before a significant increase in nuclei. The β/α

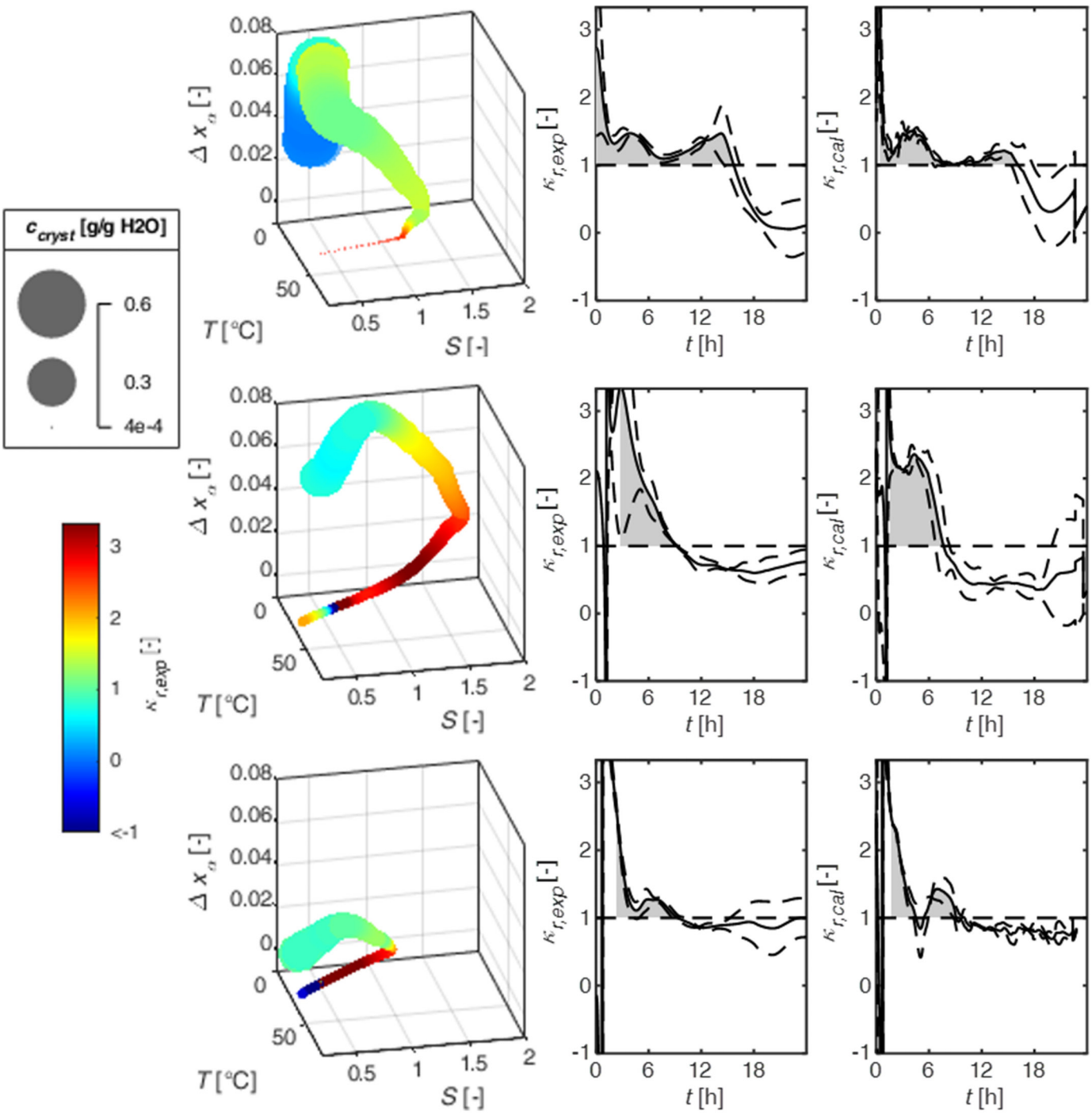

Figure 6. Regarding our 3 different experimental conditions: left: kinetic ratio $\kappa_{r,exp}$ in dependence of distance from mutarotation equilibrium Δx_α, crystal load c_{cryst}, temperature, and supersaturation, middle: experimentally determined kinetic ratio $\kappa_{r,exp}$ in dependence of time, right: kinetic ratio $\kappa_{r,cal}$ in dependence of time calculated with total lactose load data and mutarotation kinetics from the literature (McLeod, 2007). Standard deviation from 3 experimental repetitions are shown with dotted lines. Integrals from Table 4 are marked in gray.

ratio moved away from equilibrium during the course of high supersaturation and increasing available surface area. The supersaturation gradually declined, leading to a decrease in growth rate, while the mutarotation rate was unaffected. Therefore, a minimum in α-lactose fraction was evidenced in the experiments, showing as a maximum in Δx_α. Comparing the 2-step cooling and fast cooling to 10°C in Figure 6, the maximum super-

saturation was higher during the fast cooling experiment, but the maximum Δx_α was the same. In contrast, the crystal load (and consequently the crystal surface area) was much larger during 2-step cooling. This result further demonstrates that both supersaturation and crystal surface area influence mutarotation limitation. In comparison, both the degree of supersaturation and crystal load were lower during fast cooling to 25°C.

Prediction of mutarotation limitation. Of course, calibration for α- and β-lactose is quite challenging and elaborate. Therefore, we wanted to assess whether it would be possible to estimate mutarotation limitation based on total lactose concentration data alone. The kinetic ratio as a function of time is also plotted in Figure 6 for this purpose, calculated once based on lactose load and measured α-lactose fraction ($\kappa_{r,exp}$, experimentally determined kinetic ratio) and once based on total lactose load only ($\kappa_{r,cal}$, calculated kinetic ratio with mutarotation kinetics). The change in α-lactose fraction was calculated using theoretical mutarotation kinetics (Equations (3) - (7)) by solving the set of ordinary differential equations given by Equations (1) and (3) with $\frac{dc}{dt}$ calculated from experimental data. Mutarotation equilibrium is initially assumed. Despite the obvious differences, a high degree of similarity is evident when comparing both graphs for the different experiments. Regarding 2-step cooling, 3 local maxima were observed in both plots corresponding to the points of inflection in the x_α-graph in Figure 2. The same applies to our experiments on fast cooling to 25°C with 2 local maxima. To quantitatively compare the extent of mutarotation limitation between the experiments, the region between the kinetic ratio and the limit $\kappa_r = 1$ was calculated by integrating over the period when κ_r exceeds 1 (gray area in Figure 6). The size of this region can be used as a measure for the duration and intensity of the mutarotation limitation on the crystallization process. A large area indicates a strong mutarotation limitation either due to a high kinetic ratio or a kinetic ratio only slightly larger than 1 but over a prolonged period of time, whereas a smaller area suggests that mutarotation has had less of an impact. Therefore, we anticipated that 2-step cooling and rapid cooling to 10°C would result in larger areas, while fast cooling to 25°C would result in a smaller area. This assessment can help determine whether mutarotation should be taken into account during experimental analysis. The results of the integration are presented in Table 4. At the start of the experiment, mutarotation might trend toward β-lactose as the equilibrium β/α ratio increases with decreasing temperature. Due to a low growth depletion rate caused by low available surface area at the start, this leads to high kinetic ratios without actual mutarotation limitation. As a result, the lower integration limit was selected based on the criterion that the kinetic ratio should not exceed $\frac{1}{x_\alpha}$ (see Figure 1 for details). The integrated areas, including the measured α-lactose data, were in good alignment with the previous results. Similar areas for 2-step cooling and fast cooling to 10°C were calculated, and fast cooling to 25°C resulted in a calculated area, which was significantly lower than in the other 2 experiments. However, the integrated areas based on concentration data alone were less conclusive. In fast cooling, both methods yielded similar integrated areas, but the integrated area for 2-step cooling was significantly lower using concentration data alone. This is due to the fact that the lower integration bound was shifted to the right based on the results for $\kappa_{r,cal}$ to comply with the criterion that the kinetic ratio should not exceed $\frac{1}{x_\alpha}$. This discrepancy between both methods can be either attributed to measurement inaccuracies or inaccuracies in mutarotation kinetics. A possible improvement could be achieved by determining mutarotation kinetics ourselves and applying these for the rate analysis. Currently, an accurate comparison of mutarotation limitation using concentration data at our measurement accuracy and without determining mutarotation kinetics ourselves is not possible. However, the calculated areas all still confirmed mutarotation limitation during the experiments.

CONCLUSION

Previous research has controversially discussed the impact of mutarotation on the crystallization process, whereby the assumption of mutarotation equilibrium has often been made. Our hypothesis was that there is no universal answer to the question of whether mutarotation should be taken into account. Instead, the key question is determining when mutarotation becomes a relevant factor. We monitored the complex interaction among various phenomena (nucleation, growth, mutarotation) occurring during lactose crystallization from aqueous solution via ATR-FTIR and FBRM inline measurements. We demonstrated that mutarotation limits the crystallization process for certain experimental conditions. The resulting change in β/α ratio greatly affected supersaturation. To systematically address our research question we performed a theoretical analysis, as well. In conclusion, mutarotation limitation depends mainly on the level of supersaturation and crystal surface available in the crystallizer. Interestingly, the effect of temperature seems less prominent,

Table 4: Calculated area between κ_r and 1 for $\kappa_r > 1$ as an indicator for mutarotation limitation. Calculated using experimental data, including α-lactose fraction $\kappa_{r,exp}$ and with total lactose load and mutarotation kinetics from the literature (McLeod, 2007) $\kappa_{r,cal}$. Initial time interval where mutarotation trends toward β-lactose due to temperature-dependent equilibrium is excluded ($t = 0$-t_{min})

Experiment no.	$\int_{t_{min}}^{t_{max}} (\kappa_{r,exp} - 1)\ dt$ [h]	$\int_{t_{min}}^{t_{max}} (\kappa_{r,cal} - 1)\ dt$ [h]
1 - 2-step cooling	5.70	3.26
2 - Fast cooling to 10°C	6.03	6.31
3 - Fast cooling to 25°C	2.19	2.98

which can be explained by the similar activation energies found for mutarotation and growth, thus leading to similar temperature dependencies. The assumption of mutarotation equilibrium throughout the crystallization process for pure lactose-water systems is only valid under a very limited set of process conditions, e.g., at low supersaturations due to very slow cooling.

ACKNOWLEDGMENTS

This IGF Project 21342N of the FEI is supported via AiF within the program for promoting the Industrial Collective Research (IGF) of the Federal Ministry of Economic Affairs and Climate Action (BMWK), based on a resolution of the German Parliament. The OptiMax Synthesis workstation was funded by the Deutsche Forschungsgemeinschaft (DFG) through grant INST 95/1299.

Data availability statement The raw data can be made available by the authors upon request without undue reservation. Inquiries can be directed to the corresponding author.

REFERENCES

Altamimi, M. J., K. Wolff, A. Nokhodchi, G. P. Martin, and P. G. Royall. 2019. Variability in the α and β anomer content of commercially available lactose. Int. J. Pharm. 555:237–249. https://doi.org/10.1016/j.ijpharm.2018.10.061.

Arellano, M. P., J. M. Aguilera, and P. Bouchon. 2004. Development of a digital video-microscopy technique to study lactose crystallisation kinetics in situ. Carbohydr. Res. 339:2721–2730. https://doi.org/10.1016/j.carres.2004.09.009.

Binel, P., A. Jain, A. Jaeggi, D. Biri, A. K. Rajagopalan, A. J. deMello, and M. Mazzotti. 2023. Online 3D Characterization of Micrometer-Sized Cuboidal Particles in Suspension. Small Methods 7:e2201018. https://doi.org/10.1002/smtd.202201018.

Borchert, C., and K. Sundmacher. 2012. Morphology evolution of crystal populations: Modeling and observation analysis. Chem. Eng. Sci. 70:87–98. https://doi.org/10.1016/j.ces.2011.05.057.

Buma, T. J., and H. K. C. van der Keen. 1974. Accurate specific optical rotations of lactose, and their dependence on temperature. Neth. Milk Dairy J. 175–185.

Chandrapala, J., R. Wijayasinghe, and T. Vasiljevic. 2016. Lactose crystallization as affected by presence of lactic acid and calcium in model lactose systems. J. Food Eng. 178:181–189. https://doi.org/10.1016/j.jfoodeng.2016.01.019.

Cornel, J., C. Lindenberg, and M. Mazzotti. 2008. Quantitative Application of in Situ ATR-FTIR and Raman Spectroscopy in Crystallization Processes. Ind. Eng. Chem. Res. 47:4870–4882. https://doi.org/10.1021/ie800236v.

Darmali, C., S. Mansouri, N. Yazdanpanah, and M. W. Woo. 2021. Cooling crystallization of lactose in the presence of whey protein and lactic acid impurities. J. Food Eng. 311:110729. https://doi.org/10.1016/j.jfoodeng.2021.110729.

Dincer, T. D., M. I. Ogden, and G. M. Parkinson. 2009. In situ investigation of growth rates and growth rate dispersion of α-lactose monohydrate crystals. J. Cryst. Growth 311:1352–1358. https://doi.org/10.1016/j.jcrysgro.2009.01.016.

Eder, C., C. Choscz, V. Müller, and H. Briesen. 2015. Jamin-interferometer-setup for the determination of concentration and temperature dependent face-specific crystal growth rates from a single experiment. J. Cryst. Growth 426:255–264. https://doi.org/10.1016/j.jcrysgro.2015.06.012.

Frawley, P. J., N. A. Mitchell, C. T. Ó'Ciardhá, and K. W. Hutton. 2012. The effects of supersaturation, temperature, agitation and seed surface area on the secondary nucleation of paracetamol in ethanol solutions(75):183–197. https://doi.org/10.1016/j.ces.2012.03.041.

Fujiwara, M., P. S. Chow, D. L. Ma, and R. D. Braatz. 2002. Paracetamol Crystallization Using Laser Backscattering and ATR-FTIR Spectroscopy: Metastability, Agglomeration, and Control. Cryst. Growth Des. 2:363–370. https://doi.org/10.1021/cg0200098.

Gernigon, G., F. Baillon, F. Espitalier, C. Le Floch-Fouéré, P. Schuck, and R. Jeantet. 2013. Effects of the addition of various minerals, proteins and salts of organic acids on the principal steps of α-lactose monohydrate crystallisation. Int. Dairy J. 30:88–95. https://doi.org/10.1016/j.idairyj.2012.12.005.

Haase, G., and T. A. Nickerson. 1966a. Kinetic Reactions of Alpha and Beta Lactose. I. Mutarotation. J. Dairy Sci. 49:127–132. https://doi.org/10.3168/jds.S0022-0302(66)87811-6.

Haase, G., and T. A. Nickerson. 1966b. Kinetic Reactions of Alpha and Beta Lactose. II. Crystallization. J. Dairy Sci. 757–761:757–761. https://doi.org/10.3168/jds.S0022-0302(66)87941-9.

Herrington, B. L. 1934a. Some Physico-Chemical Properties of Lactose: I. The Spontaneous Crystallization of Supersaturated Solutions of Lactose. J. Dairy Sci. 17:501–518. https://doi.org/10.3168/jds.S0022-0302(34)93265-3.

Herrington, B. L. 1934b. Some Physico-Chemical Properties of Lactose: IV. The Influence of Salts and Acids upon the Mutarotation Velocity of Lactose. J. Dairy Sci. 17:659–670. https://doi.org/10.3168/jds.S0022-0302(34)93285-9.

Höving, S., L. Neuendorf, T. Betting, and N. Kockmann. 2023. Determination of Particle Size Distributions of Bulk Samples Using Micro-Computed Tomography and Artificial Intelligence. Materials (Basel) 16:1002. https://doi.org/10.3390/ma16031002.

Huo, Y., T. Liu, Y. Yang, C. Y. Ma, X. Z. Wang, and X. Ni. 2020. In Situ Measurement of 3D Crystal Size Distribution by Double-View Image Analysis with Case Study on l -Glutamic Acid Crystallization. Ind. Eng. Chem. Res. 59:4646–4658. https://doi.org/10.1021/acs.iecr.9b05828.

Jawad, R., A. F. Drake, C. Elleman, G. P. Martin, F. J. Warren, B. B. Perston, P. R. Ellis, M. A. Hassoun, and P. G. Royall. 2014. Stability of sugar solutions: a novel study of the epimerization kinetics of lactose in water. Mol. Pharm. 11:2224–2238. https://doi.org/10.1021/mp400509t.

Jelen, P., and S. T. Coulter. 1973. Effects of supersaturation and temperature on the growth of lactose crystals. J. Food Sci. 38:1182–1185. https://doi.org/10.1111/j.1365-2621.1973.tb07233.x.

Jenness, R., and J. Koops. 1962. Preparation and properties of a salt solution which simulates milk ultrafiltrate. Neth. Milk Dairy J. ●●●:16.

Kačuráková, M., and M. Mathlouthi. 1996. FTIR and laser-Raman spectra of oligosaccharides in water: characterization of the glycosidic bond. Carbohydr. Res. 284:145–157. https://doi.org/10.1016/0008-6215(95)00412-2.

Kendrew, J. C., and E. A. Moelwyn-Hughes. 1940. The Kinetics of Mutarotation in Solution. Proceeding of the Royal Society of London. Series A(176 (966)):352–367. https://doi.org/10.1098/rspa.1940.0094.

Knowles, I., and R. J. Renka. 2014. Variational and Topological Methods: Theory, Applications, Numerical Simulations, and Open Problems (2012). Electronic Journal of Differential Equations(Conference 21):235–246.

Lewiner, F., J. P. Klein, F. Puel, and G. Fevotte. 2001. On-line ATR FTIR measurement of supersaturation during solution crystallization processes. Calibration and applications on three solute/solvent systems. Chem. Eng. Sci. 56:2069–2084. https://doi.org/10.1016/S0009-2509(00)00508-X.

Lins, J., T. Harweg, F. Weichert, and K. Wohlgemuth. 2022. Potential of Deep Learning Methods for Deep Level Particle Characterization in Crystallization. Appl. Sci. (Basel) 12:2465. https://doi.org/10.3390/app12052465.

López-Pablos, A. L., C. C. Leyva-Porras, M. B. Silva-Cázares, F. E. Longoria-Rodríguez, S. A. Pérez-García, Á. A. Vértiz-Hernández, and M. Z. Saavedra-Leos. 2018. Preparation and Characterization of High Purity Anhydrous β -Lactose from α -Lactose Monohydrate at Mild Temperature. Int. J. Polym. Sci. 2018:1–10. https://doi.org/10.1155/2018/5069063.

McLeod, J. 2007. Nucleation and growth of alpha lactose monohydrate. Dissertation.

McSweeney, P., and P. F. Fox. 2009. Advanced Dairy Chemistry. Springer New York, New York, NY.

Miloudi, L., F. Bonnier, K. Barreau, D. Bertrand, X. Perse, F. Yvergnaux, H. J. Byrne, I. Chourpa, and E. Munnier. 2018. ATR-IR coupled to partial least squares regression (PLSR) for monitoring an encapsulated active molecule in complex semi-solid formulations. Analyst (Lond.) 143:2377–2389. https://doi.org/10.1039/C8AN00547H.

Mimouni, A., P. Schuck, and S. Bouhallab. 2009. Isothermal batch crystallization of alpha-lactose: A kinetic model combining mutarotation, nucleation and growth steps. Int. Dairy J. 19:129–136. https://doi.org/10.1016/j.idairyj.2008.09.006.

Nagy, Z. K., and R. D. Braatz. 2012. Advances and new directions in crystallization control. Annu. Rev. Chem. Biomol. Eng. 3:55–75. https://doi.org/10.1146/annurev-chembioeng-062011-081043.

Nagy, Z. K., M. Fujiwara, and R. D. Braatz. 2008. Modelling and control of combined cooling and antisolvent crystallization processes. J. Process Contr. 18:856–864. https://doi.org/10.1016/j.jprocont.2008.06.002.

Neoptolemou, P., N. Goyal, A. J. Cruz-Cabeza, A. A. Kiss, D. J. Milne, and T. Vetter. 2022. A novel image analysis technique for 2D characterization of overlapping needle-like crystals. Powder Technol. 399:116827. https://doi.org/10.1016/j.powtec.2021.09.017.

Pandalaneni, K., and J. K. Amamcharla. 2016. Focused beam reflectance measurement as a tool for in situ monitoring of the lactose crystallization process. J. Dairy Sci. 99:5244–5253. https://doi.org/10.3168/jds.2015-10643.

Pandalaneni, K., and J. K. Amamcharla. 2018. Evaluating the crystallization of lactose at different cooling rates from milk and whey permeates in terms of crystal yield and purity. J. Dairy Sci. 101:8805–8821. https://doi.org/10.3168/jds.2018-14846.

Patel, K. N., and T. A. Nickerson. 1970. Influence of Sucrose on the Mutarotation Velocity of Lactose. J. Dairy Sci. 53:1654–1658. https://doi.org/10.3168/jds.S0022-0302(70)86458-X.

Paterson, A. 2016. Lactose processing: from fundamental understanding to industrial application. Int. Dairy J. 67:80–90. https://doi.org/10.1016/j.idairyj.2016.07.018.

Paterson, A. H. J. 2009. Production and Uses of Lactose. p. 105–120. *In* P. McSweeney, and P. F. Fox (eds.). Advanced Dairy Chemistry. Springer New York, New York, NY.

Rachah, A., and D. Noll. 2015. Modeling and control of a semi-batch cooling seeded crystallizer. 6th International Conference on Modeling, Simulation, and Applied Optimization (ICMSAO):1–6. https://doi.org/10.1109/ICMSAO.2015.7152213.

Raghavan, S. L., R. I. Ristic, D. B. Sheen, and J. N. Sherwood. 2001. The bulk crystallization of alpha-lactose monohydrate from aqueous solution. J. Pharm. Sci. 90:823–832. https://doi.org/10.1002/jps.1036.

Roetman, K., and T. J. Buma. 1974. Temperature dependence of the eqilibrium β/α ratio of lactose in aqueous solution. Neth. Milk Dairy J. 155–165.

Sánchez-García, Y. I., N. Gutiérrez-Méndez, I. Salmerón, V. H. Ramos-Sánchez, M. Y. Leal-Ramos, and D. R. Sepúlveda. 2021. Mutarotation and solubility of lactose as affected by carrageenans. Food research international (Ottawa, Ont.) 142:110204. https://doi.org/10.1016/j.foodres.2021.110204.

Schiele, S. A., F. Antoni, R. Meinhardt, and H. Briesen. 2021. Analysis of Nonideal Shape Evolution during Potash Alum Crystallization Using Microcomputed Tomography and Three-Dimensional Image Analysis. Cryst. Growth Des. 21:1751–1761. https://doi.org/10.1021/acs.cgd.0c01644.

Schiele, S. A., R. Bier, A. Ommert, and H. Briesen. 2023. Direct Crystal Growth Control: Controlling Crystallization Processes by Tracking an Analogue Twin. Ind. Eng. Chem. Res. 62:5491–5501. https://doi.org/10.1021/acs.iecr.2c04648.

Schiele, S. A., R. Meinhardt, C. Eder, and H. Briesen. 2020. ATR-FT-IR spectroscopy for in-line anomer concentration measurements in solution: A case study of lactose. Food Control 110:107024. https://doi.org/10.1016/j.foodcont.2019.107024.

Shi, Y., R. W. Hartel, and B. Liang. 1989. Formation and Growth Phenomena of Lactose Nuclei Under Contact Nucleation Conditions. J. Dairy Sci. 72:2906–2915. https://doi.org/10.3168/jds.S0022-0302(89)79441-8.

Shi, Y., B. Liang, and R. W. Hartel. 1990. Crystallization Kinetics of Alpha-Lactose Monohydrate in a Continuous Cooling Crystallizer. J. Food Sci. 55:817–820. https://doi.org/10.1111/j.1365-2621.1990.tb05238.x.

Simone, E., A. I. I. Tyler, D. Kuah, X. Bao, M. E. Ries, and D. Baker. 2019. Optimal Design of Crystallization Processes for the Recovery of a Slow-Nucleating Sugar with a Complex Chemical Equilibrium in Aqueous Solution: The Case of Lactose. Org. Process Res. Dev. 23:220–233. https://doi.org/10.1021/acs.oprd.8b00323.

Töpel, A. 2016. Chemie und Physik der Milch: Naturstoff, Rohstoff, Lebensmittel. 4. überarbeitete Auflage. Behr's Verlag, Hamburg.

Troy, H. C., and P. F. Sharp. 1930. α and β lactose in some milk products. J. Dairy Sci. 13(XIII (2)):140–157. https://doi.org/10.3168/jds.S0022-0302(30)93513-8.

Twieg, W. C., and T. A. Nickerson. 1968. Kinetics of Lactose Crystallization. J. Dairy Sci. 51:1720–1724. https://doi.org/10.3168/jds.S0022-0302(68)87265-0.

van Krevald, A. 1969. Growth Rates of Lactose Crystals in Solutions of Stable Anhydrous alpha-Lactose. Neth. Milk Dairy J. 258–274.

van Kreveld, A., and A. S. Michaels. 1965. Measurement of Crystal Growth of -Lactose. J. Dairy Sci. 48:259–265. https://doi.org/10.3168/jds.S0022-0302(65)88213-3.

Visser, R. A. 1982. Supersaturation of α-lactose in aqueous solutions in mutarotation equilibrium. Neth. Milk Dairy J. ●●●:36.

Vu, T., R. J. Durham, J. A. Hourigan, and R. W. Sleigh. 2006. Dynamic modelling optimisation and control of lactose crystallisations: Comparison of process alternatives. Separ. Purif. Tech. 48:159–166. https://doi.org/10.1016/j.seppur.2005.07.015.

Wijayasinghe, R., D. Bogahawaththa, J. Chandrapala, and T. Vasiljevic. 2020. Crystallization behavior and crystal properties of lactose as affected by lactic, citric, or phosphoric acid. J. Dairy Sci. 103:11050–11061. https://doi.org/10.3168/jds.2020-18375.

Wong, S. Y., R. K. Bund, R. K. Conelly, and R. W. Hartel. 2012. Designing a lactose crystallization process based on dynamic metastable limit. J. Food Eng. 111:642–654. https://doi.org/10.1016/j.jfoodeng.2012.03.003.

Wong, S. Y., and R. W. Hartel. 2014. Crystallization in lactose refining-a review. J. Food Sci. 79:R257–R272. https://doi.org/10.1111/1750-3841.12349.

Woo, X. Y., Z. K. Nagy, R. B. H. Tan, and R. D. Braatz. 2009. Adaptive Concentration Control of Cooling and Antisolvent Crystallization with Laser Backscattering Measurement. Cryst. Growth Des. 9:182–191. https://doi.org/10.1021/cg800131r.

Zeng, X. M., G. P. Martin, C. Marriott, and J. Pritchard. 2000. The influence of crystallization conditions on the morphology of lactose intended for use as a carrier for dry powder aerosols. J. Pharm. Pharmacol. 52:633–643. https://doi.org/10.1211/0022357001774462.

Zhou, G. X., M. Fujiwara, X. Y. Woo, E. Rusli, H.-H. Tung, C. Starbuck, O. Davidson, Z. Ge, and R. D. Braatz. 2006. Direct Design of Pharmaceutical Antisolvent Crystallization through Concentration Control. Cryst. Growth Des. 6:892–898. https://doi.org/10.1021/cg0504049.

ORCIDS

Ramona Bier https://orcid.org/0000-0002-8559-7429
Cornelia Eder https://orcid.org/0009-0005-1397-7819
Simon A. Schiele https://orcid.org/0000-0003-3026-2768
Heiko Briesen https://orcid.org/0000-0001-7725-5907

APPENDIX

Anomer content determination via polarimetry

Polarimetry was used to determine the β/α ratio in the original lactose powders which were used for calibration. Additionally, the β/α ratio was also analyzed in solution samples obtained from the crystallization experiments for validation purposes (see section 6.5). A P800-PT polarimeter with temperature control and 589 nm wavelength from Krüss Optronic GmbH, Germany was used. The optical rotation values provided by the polarimeter need to be converted to specific rotation values via division of concentration in g lactose anhydride per 100 mL of solution and multiplication with optical path length. The exact lactose concentration c in the powder is unknown beforehand, as the amount of α-lactose monohydrate and, therefore, hydrate in the powder is not known. Therefore, the concentration value needs to be calculated from polarimetry measurement as well. In this case, the specific optical rotation at equilibrium (Töpel, 2016) can be used:

$$[\alpha]^{T}_{589\,\mathrm{nm}} = 55.23 - 0.01688 \cdot \frac{c}{\mathrm{g}\,/\,100\,\mathrm{mL}} - 0.07283 \cdot \left(\frac{T - 273.15}{^{\circ}C} - 25\right). \quad (19)$$

Given that the concentration was far below saturation, the dissolution of lactose in water was fast (≤40 s). The initial time t_0 was defined as the point at which the solution became visibly clear. In case of solution samples, time was started after the first measurement. The change in α-lactose fraction x_α at constant concentration can be described using Equation (5). The specific optical rotation $[\alpha]^{20\,^{\circ}C}_{589\,nm}$ determined via polarimetry is the sum of both α- and β-lactose optical rotation (Töpel, 2016; Haase and Nickerson, 1966a).

$$[\alpha]^{20\,^{\circ}\mathrm{C}}_{589\,\mathrm{nm}} = 88^{\circ} \cdot x_\alpha(t) + 32.6^{\circ} \cdot [1 - x_\alpha(t)] \quad (20)$$

Combining the 3 equations, the mass fraction of α-lactose at initial time and concentration can be regressed from the data curve. For dry powder analysis, 0.45 g of powder was dissolved in 100 g water at 20°C. The analysis of pharmaceutical-grade lactose from Sigma Aldrich yielded $x_\alpha = 1$. The result was in good agreement with results by Altamimi et al. (2019), who measured $x_\alpha = 0.984$ for Sigma Aldrich lactose via H-NMR.

Density measurements

The density of lactose solution is used to convert lactose load into molar concentration. Density was measured with a DM40 density meter from Mettler Toledo Inc., U.S.A. Density was measured for different lactose loads c (g lactose anhydride per g of water) and temperatures T to generate an empirical correlation for density ρ_{liq} of pure lactose –water (Eq. (22), $R^2 = 0.998$).

$$\frac{\rho_{liq}}{\left[\mathrm{g}\,/\,\mathrm{cm}^3\right]} = 1.0123 + 0.3476 \cdot \frac{c}{\left[\mathrm{g}\,/\,\mathrm{g}\right]} - 0.1038 \cdot \left(\frac{c}{\left[\mathrm{g}\,/\,\mathrm{g}\right]}\right)^2 - 0.5068 \cdot 10^{-3} \cdot \frac{T}{[^{\circ}C]}. \quad (21)$$

Refractometry

Lactose concentration during calibration and validation was measured via refractometry. A DR600-T and a DR6200-T refractometer (Krüss Optronic GmbH, Germany) was used to measure refractive indices. A linear calibration curve for lactose hydrate mass fraction w was obtained at 25°C with $R^2 = 0.999$, root mean square error = 0.003:

$$w = 5.6915 \cdot RI - 7.5515. \quad (22)$$

ATR-FTIR calibration

Calibration spectra were obtained in the range of 0.07–1.3 g lactose anhydride/g water and 10–90°C as shown in Figure 7. α-lactose monohydrate and demineralized water were mixed in the reactor to achieve the desired concentration and heated above solubility temperature for the lactose to completely dissolve. Afterward, the solution was cooled to the desired temperature and held until mutarotation equilibrium was reached, as calculated by Equation (5) or nucleation occurred. Nucleation was detected visually and via a drop in the characteristic peak height at 1037 cm^{-1}, which is independent of β/α ratio (Schiele et al., 2020), see Figure 8). Data points where nucleation occurred were excluded from the calibration set. In addition, calibration experiments were conducted by heating a mixture of 0.3, 0.5, and 0.7 g/g lactose load from 10°C to 80°C as rapidly as possible (using our reactor setup approximately 40 min) and cooled again to 10°C. Due to fast cooling/heating, mutarotation equilibrium cannot be achieved at every temperature during the course of the temperature ramp, and mutarotation states were calculated according to Equation (5). Calibration spectra at different β/α ratios were obtained directly after addition of α- or β-lactose in an undersaturated solution at 0.05–0.12 g/g and 10–50°C since the crystals dissolved within one measuring period. Spectra were then continuously acquired until mutarotation equilibrium was achieved. The 2 anomers were incorporated as 2 separate components in the PLS model. According to Lambert Beer's Law, molar concentration is proportional to absorption. It is hence reasonable to convert loads to molar concentration for linearization before training. The molar concentration was calculated from the load c with the density from Equation (21) and the molar mass of lactose anhydrite $M_{Lac} = 342.3$ g/mol.

$$c_{mol} = \frac{c}{c+1} \cdot \frac{\rho_{liq}}{M_{Lac}}. \quad (23)$$

The region of 1200–950 cm^{-1} of the FTIR spectra was used for model building. Characteristic peaks corresponding to stretching and bending modes of CH-, CO- and OH- bonds of different oligosaccharides can be assigned to this region (Kačuráková and Mathlouthi, 1996). Lactose also exhibits distinct bands in this region. The stretching and vibrational modes of the C-O-C glycosidic bond of lactose in particular can be assigned to this region (López-Pablos et al., 2018). The ATR-FTIR data in Figure 8 show 2 exemplary lactose spectra at high and low β/α ratios. Figure 8 illustrates that distinct peaks at 1096 and 1033 cm^{-1} can be attributed to α-lactose, while at 1078 and 1043 cm^{-1} characteristic bands of β-lactose were observed. The spectra were in good agreement with measurements by (Jawad et al., 2014), with the respective peaks at 1099 and 1031 cm^{-1} for lactose with low β/α ratio and 1076 and 1043 cm^{-1} for lactose at a high β/α ratio. For multivariate regression, 191 spectra were used as training set, and 68 were used as a test set for the PLS model. Several data preprocessing steps were tested, e.g., baseline correction, smoothing, and derivatives. Using the spectral region of 1200–950 cm^{-1} and applying the first derivative, and neither smoothing nor base line correction yielded the best results regarding root mean square error of calibration data (**RMSEC**), cross validation (**RMSECV**), and prediction (**RMSEP**). Mean centering and variance scaling were also applied as further standard preprocessing steps. The number of latent variables (**LV**) considered in the PLS model is a crucial factor for prediction performance. Too many LVs will result in overfitting the model. If too few LVs are chosen, the model will not be able to distinguish α- and β-lactose. The RMSECV is often used as a tool for determining the number of latent variables. The optimal number is considered to be the minimum of RMSECV in dependence of the number of latent variables (Cornel et al., 2008; Miloudi et al., 2018). In our case 6 LV were chosen.

PLS Model validation

For validation purposes, samples were taken throughout the experiments and analyzed via refractometer and polarimetry, which was in addition to the statistical validation via cross validation and test set described in the previous section. Samples were taken from the center of the reactor with a pipette and quickly filtered with a funnel and Macherey-Nagel MN616 filter paper. In the case of polarimetry, the samples were immediately transferred to sample tubes, which were placed in an ice bath to cool the sample and decelerate further mutarotation. Polarimetry measurements were started within 5 min after sampling. External polarimetry measurement was performed for 45 min at a 30 s measurement interval. Measurements are shown for parameter settings 1 and 2 from Table 1 for one repetition each. 95% confidence intervals were calculated from the RMSEP of ATR-FTIR and refractometry and from regression analysis for polarimetry. Good agreement was evident for concentration and polarimetry measurement from Figure 9. With 90 measurement points over 45 min for the regression, accuracy of polarimetry was within the

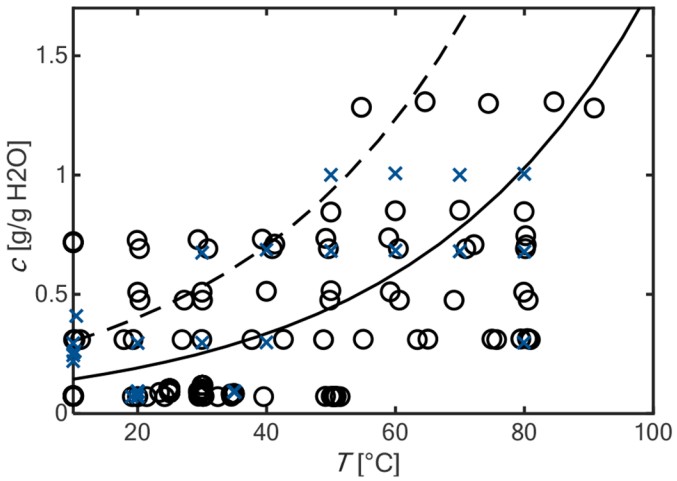

Figure 7. Calibration points for the PLS model: Training data (o), test data (x). The solubility curve is indicated as solid line and the metastable boundary indicated as a dashed line, accordig to McLeod (2007).

same range as with ATR-FTIR. This result did not take measurement error into consideration due to the sample preparation time. In addition, at least 15 mL of sample were needed for each measurement, making it infeasible to take continuous samples throughout the experiment.

Effect of CIP procedure

Lactose crystals tend to deposit or nucleate within the probe window of the ATR-FTIR spectroscope. Crystalline α-lactose monohydrate has absorption bands in the same wavelength range as dissolved lactose (see Figure 10). CIP procedure included temporal reduction of stirrer speed and, thus, a steep increase in temperature at the ATR-FTIR probe tip leading to a quick dissolution of deposited solids. This affected the measurement via temporal higher concentration and temperature in the measurement area. Reactor temperature deviated by maximum ± 0.5°C during the course of CIP. A temporal decrease in particle counts was visible in the FBRM data, indicating partial sedimentation (see Figure 11). However, partial sedimentation does not seem to induce agglomeration at the bottom of the vessel, as indicated by a chord length distribution comparison before and after CIP cycles. No CIP procedure influence was observed regarding concentration trends during repetitive experimental runs, although the number and timing of CIP cycles did vary.

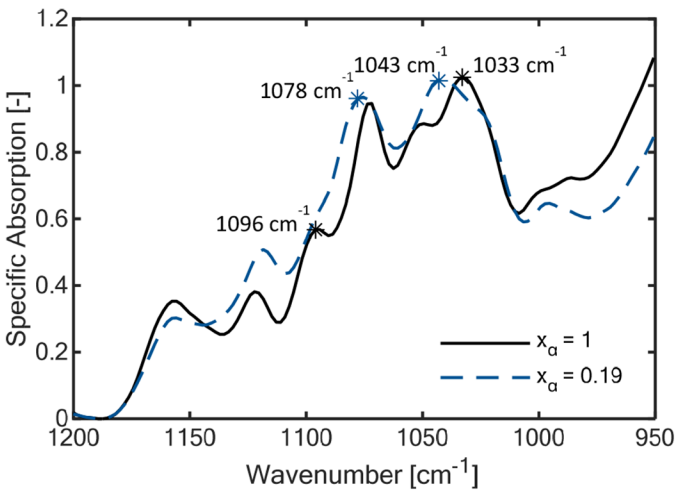

Figure 8. ATR-FTIR spectra of lactose at 20°C and 0.07 g/g with $x_\alpha = 1$ (solid black) and $x_\alpha = 0.19$ (dashed blue). A baseline correction at 1189 cm^{-1} and normalization at 1037 cm^{-1} were performed.

Yield calculation

The yield is calculated as mass of lactose crystallized in relation to total mass of lactose, which can be written as:

$$Y = \frac{m_{H2O,0} \cdot c_0 - m_{H2O,end} \cdot c_{end}}{m_{H2O,0} \cdot c_0}. \quad (24)$$

With mass of water m_{H2O} and lactose load c. The index *0* marks the values at initial time $t = 0$ and *end* marks the values at final time $t = 24$ h. As water is incorporated into the crystal lattice, the amount of liquid water is not constant and can be calculated according to:

$$m_{H2O,end} = \frac{m_{H2O,0} - \frac{0.05}{0.95} \cdot m_{H2O,0} \cdot c_0}{1 - \frac{0.05}{0.95} \cdot c_{end}}. \quad (25)$$

This yield is a temperature-independent measure to quantify how much of total lactose present is recovered by crystallization.

Growth kinetics

To determine the equation for the growth rate of the (010) facet as a function of α-lactose concentration and temperature, experiments were carried out with lactose monohydrate crystals in aqueous solution using the experimental set-up and the temperature profile described in Eder et al. (2015). To cover a significant concentration range during the 24-h temperature rests, 2 crystals were mounted in the growth chamber. Furthermore, 2 experiments with different starting concentrations

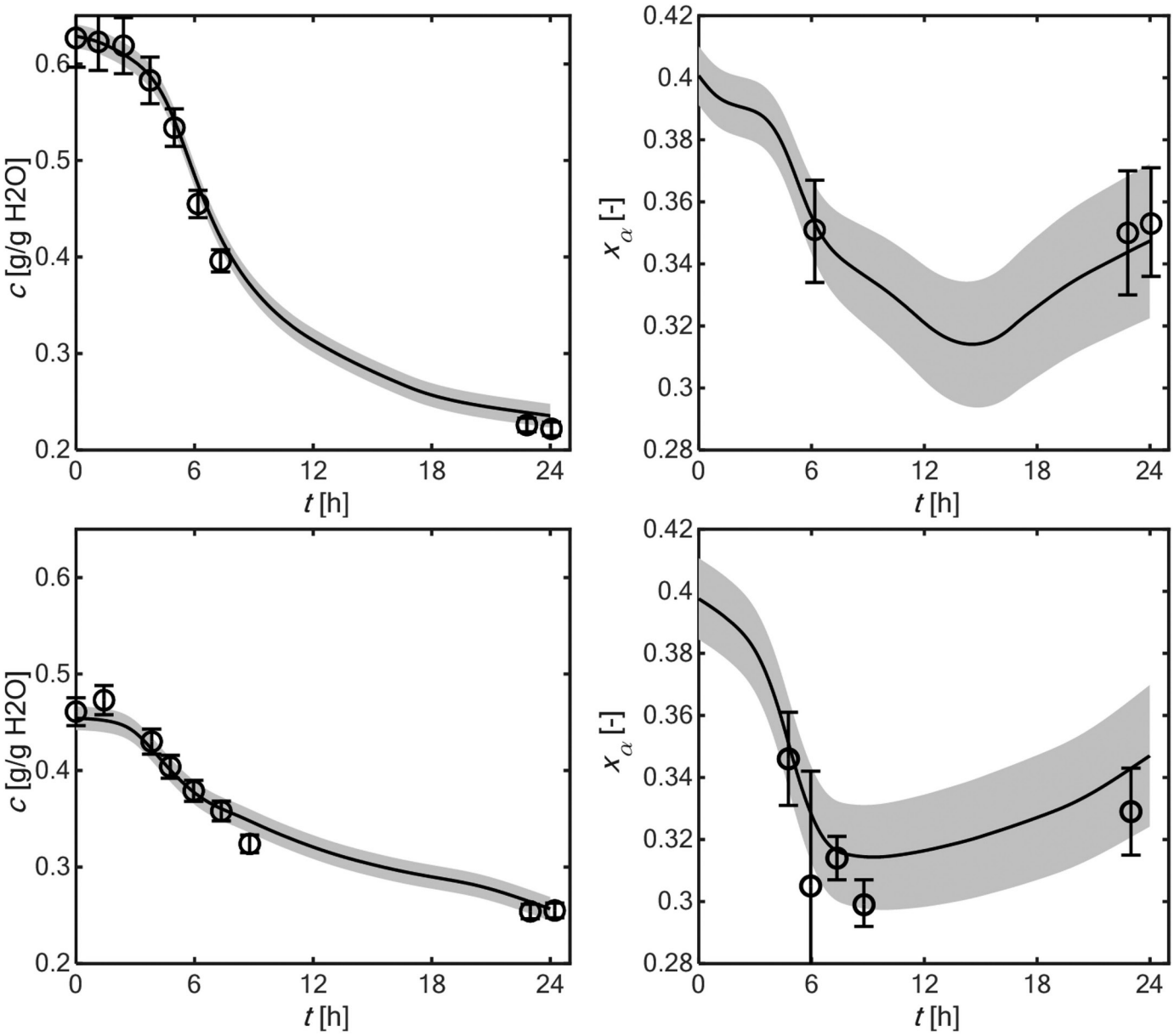

Figure 9. Left: Lactose load and right: α-lactose fraction measured via ATR-FTIR regularized (line) and via offline refractometry and polarimetry (o) during one experimental run under process conditions 1 (top) and 2 (bottom). 95% confidence intervals are indicated in gray for continuous measurement and as error bars for offline analysis.

of 0.54 and 0.47 g lactose anhydride/g H_2O were performed. The determination of the position of the (010) facet as well as the current total lactose concentration at the phase boundary was carried out as described in Eder et al. (2015). The contrast factor $dn/dc = 0.0863$ was used to convert the displacement of interference fringes into the spatially and time-resolved lactose concentration. Beginning with the starting concentration c_0, the concentration c_i is calculated using the equation

$$c_i = c_{i-1} + \frac{\Delta n_{i,i-1}}{dn/dc}, \tag{26}$$

with the index i indicating the number of the image.

Figure 12 shows the results for the experiment with the higher starting concentration. Although the 2 crystals grew close together in the same cell and the concentration at the phase boundary was almost identical, the growth rates differed significantly. In Eder et al.

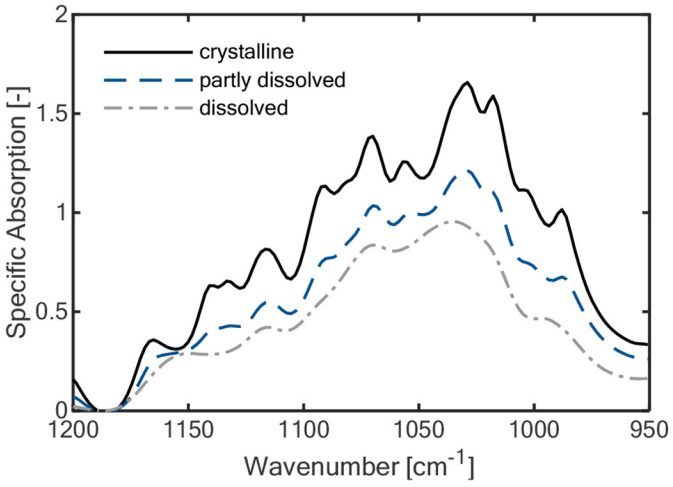

Figure 10. ATR-FTIR spectra of crystalline lactose, partial fouling and dissolved lactose. A baseline correction at 1189 cm^{-1} was performed.

(2015), lactose growth was studied in an aqueous solution containing 0.3 mol KCl/kg H_2O. The salt content accelerates the mutarotation, so mutarotation equilibrium could be assumed for the further evaluation. Mutarotation is slower in salt-free solution. Equilibrium cannot be assumed, especially after the temperature ramps. Therefore, the α-lactose supersaturation must be used to calculate the growth rate. Since only the total lactose content can be read from the interferometric measurement, the α-lactose content had to be determined based on the total lactose concentration, considering mutarotation and crystal growth kinetics. Beginning with mutarotation equilibrium, that was established after the 60°C phase of the temperature profile, the changes in α- and β-lactose concentrations were calculated based on Equations (1) and (3). The reduction of α-lactose due to crystal growth corresponds to the measured decrease in the total lactose concentration and was, therefore, obtained from experimental data. The set of ordinary differential equations constituting Equations (1) and (3) was solved with finite differences applying the mutarotations kinetics from Equations (6) and (7). The α-lactose concentration is then converted to supersaturation according to Equations (12) - ((16). Figure 13 illustrates the calculated β/α ratio and the α-lactose-supersaturation during the experiment that was shown in Figure 12. Especially during the low temperature rest, the α-lactose content was clearly lower than in mutarotation equilibrium. For each of the 3 temperature rests, the growth rate G as a function of the supersaturation was determined in a fitting procedure that included all 4 of the crystals investigated. The position of the crystal surface L was fitted by:

$$L_i = L_{i-1} + G_i \cdot (t_i - t_{i-1}). \tag{27}$$

with the index i indicating the number of the image and the model equation

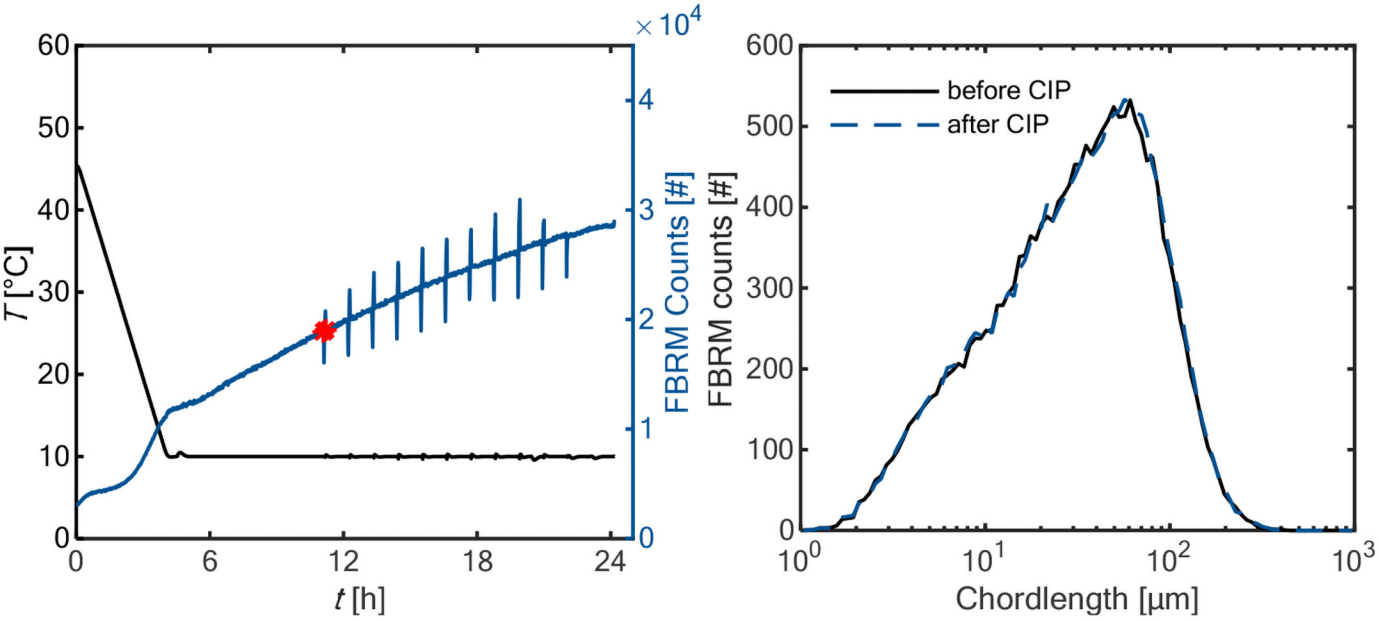

Figure 11. Left: Temperature profile and focused beam reflectance measurement (**FBRM**) total counts of one repetition of experimental run 2. Right: Chord length distribution (**CLD**) before and after first CIP procedure (time points of CLDs are marked in red in the left graph)

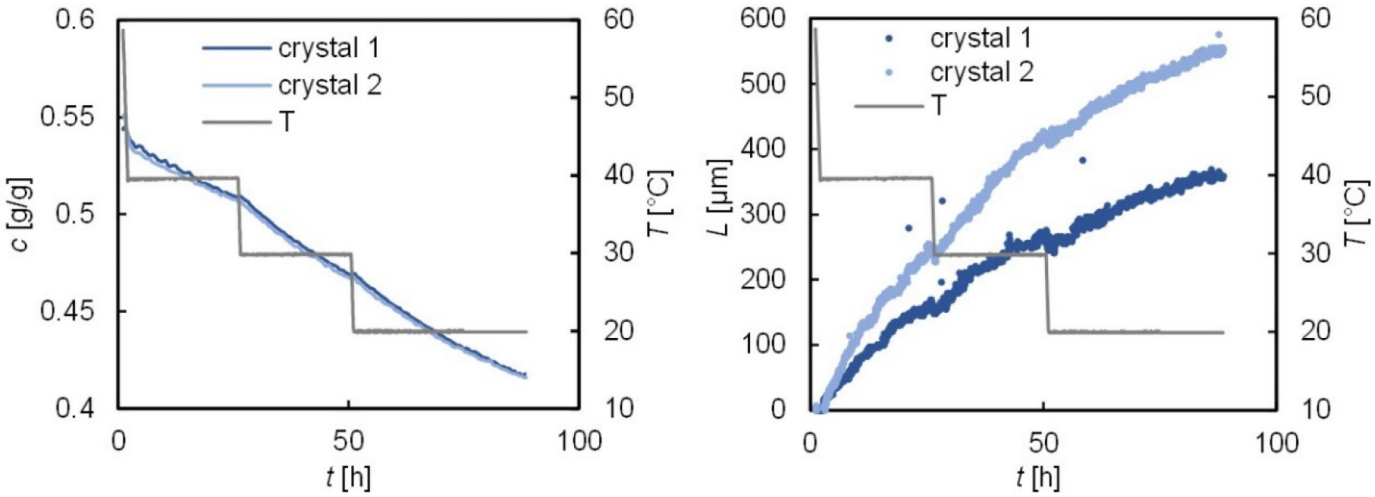

Figure 12. Typical experiment according to Eder et al. (2015). Growth of the (010) facet of 2 lactose crystals in aqueous lactose solution (starting concentration: 0.54 g/g). Left: total lactose load at crystal surface, right: face displacement.

$$G_i = k_T S_i^g, \tag{28}$$

with parameters k_T and g describing the growth rate at constant temperature. By combining the data from the experiment with 0.54 g/g starting concentration (shown in Figure 12 and Figure 13) with the data from the experiment starting at 0.47 g/g, the supersaturation and growth rates measured during the temperature rest at 40°C covered a sufficiently large range for a significant determination of g. This was not the case during the rests at the lower temperatures. The value $g = 1.8$ found at 40°C was, therefore, used as a fixed parameter for determining k_T at 20 and 30°C. The k_T values (2.006 (20°C), 6.436 (30°C) and 19.707 µm/h (40°C)) were regressed in a further step using an Arrhenius approach. The supersaturation and temperature dependency of the growth rate of the (010) facet can thus be described with the following equation:

$$G = 6.80 \cdot 10^{15} \frac{\mu m}{h} \cdot \exp\left(\frac{-87 \frac{kJ}{mol}}{RT}\right) \cdot S^{1.8}. \tag{29}$$

Figure 14 left shows the parity plots for the 4 investigated crystals. The predicted growth is in the right range. Given to the deviation between the individual

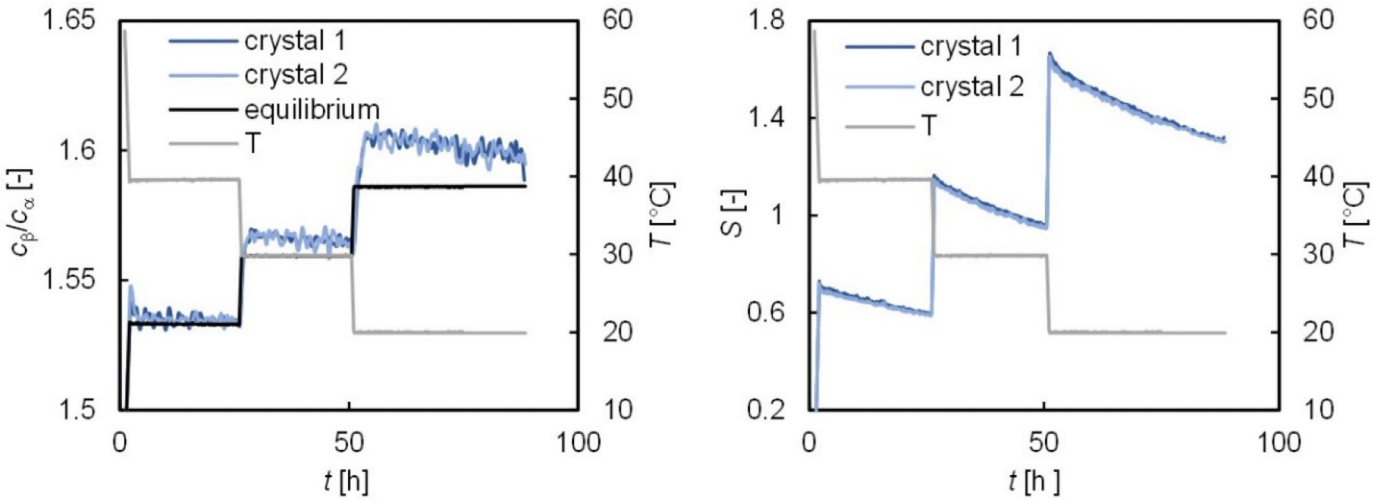

Figure 13. α-lactose content at crystal surface during the experiment presented in Figure 12. Left: β/α-ratio in comparison with the β/α-ratio in mutarotation equilibrium, right: α-lactose-supersaturation

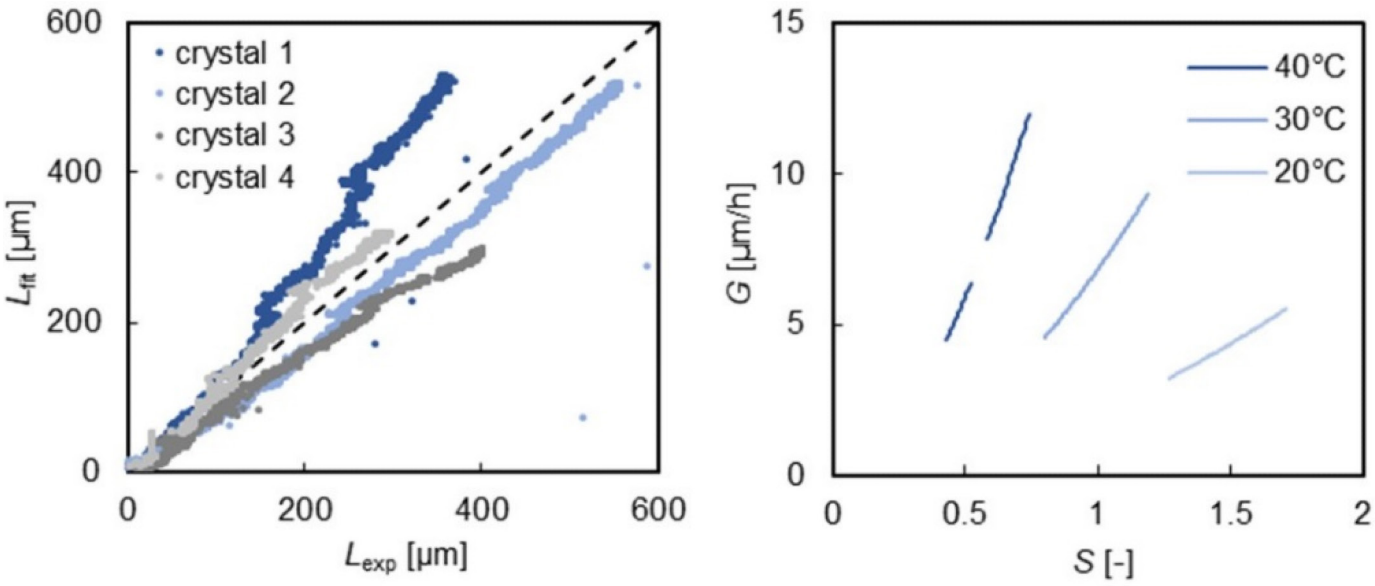

Figure 14. Growth rate of the (010) facet calculated using Equation (29): Left: comparison of measured and calculated face displacements, right: growth rate at the investigated temperatures and supersaturations.

crystals, no exact prediction was possible. Figure 14 right illustrates the temperatures and supersaturations at which the measured values were recorded and the resulting growth rates according to eq. (31). In the literature, an exponent of 2–3 is reported for growth rate (Shi et al., 1990; Arellano et al., 2004; Dincer et al., 2009) which is in alignment with our results. The activation energy is 87 kJ/mol, which matches the range of 92.5–95 kJ/mol provided by Shi et al. (1990) and Arellano et al. (2004). Dincer et al. (2009) performed measurements on the face-specific growth rate as well as mean growth rate. In their study, the mean growth rate was approximately 50–60% of (010) growth rate. However, they observed a significantly lower activation energy for (010) growth of 39.8 kJ/mol. They also compared their mean growth rate to the results of different authors (van Kreveld and Michaels, 1965; Visser, 1982; Arellano et al., 2004; Jelen and Coulter, 1973; Shi et al., 1989). Their results aligned well with the results of Shi et al. (1989) and Arellano et al. (2004) . Our growth rate of the (010) also aligns well with their mean growth rates, which is why we deem our growth rate suitable for our study. The reported growth rates of Jelen and Coulter (1973), van Kreveld and Michaels (1965) and Visser (1982) are even higher, so applying these growth rates to our theoretical analysis would lead to an even higher mutarotation limitation.